European Journal of Pharmaceutics and Biopharmaceutics 197 (2024) 114222

Contents lists available at ScienceDirect

European Journal of Pharmaceutics and Biopharmaceutics

journal homepage: www.elsevier.com/locate/ejpb

Kinetics of RNA-LNP delivery and protein expression

Judith A. Müller [a], Nathalie Schäffler [a], Thomas Kellerer [b], Gerlinde Schwake [a], Thomas S. Ligon [c], Joachim O. Rädler [a,*]

[a] Faculty of Physics and Center for NanoScience, Ludwig Maximilians-University, Munich, Germany
[b] Multiphoton Imaging Lab, Munich University of Applied Sciences, Munich, Germany
[c] Independent Researcher

A B S T R A C T

Lipid nanoparticles (LNPs) employing ionizable lipids are the most advanced technology for delivery of RNA, most notably mRNA, to cells. LNPs represent well-defined core–shell particles with efficient nucleic acid encapsulation, low immunogenicity and enhanced efficacy. While much is known about the structure and activity of LNPs, less attention is given to the timing of LNP uptake, cytosolic transfer and protein expression. However, LNP kinetics is a key factor determining delivery efficiency. Hence quantitative insight into the multi-cascaded pathway of LNPs is of interest to elucidate the mechanism of delivery. Here, we review experiments as well as theoretical modeling of the timing of LNP uptake, mRNA-release and protein expression. We describe LNP delivery as a sequence of stochastic transfer processes and review a mathematical model of subsequent protein translation from mRNA. We compile probabilities and numbers obtained from time resolved microscopy. Specifically, live-cell imaging on single cell arrays (LISCA) allows for high-throughput acquisition of thousands of individual GFP reporter expression time courses. The traces yield the distribution of mRNA life-times, expression rates and expression onset. Correlation analysis reveals an inverse dependence of gene expression efficiency and transfection onset-times. Finally, we discuss why timing of mRNA release is critical in the context of codelivery of multiple nucleic acid species as in the case of mRNA co-expression or CRISPR/Cas gene editing.

1. Introduction

Lipid nanoparticles (LNPs) provide a facilitating platform for mRNA-based delivery [1–3]. The tremendous success of mRNA based vaccination during the SARS-CoV2 pandemic also boosted the perspectives of mRNA-LNP-based therapies in a wide range of applications, including cancer immunotherapies [4,5], CAR-T cell-based immunotherapies [6] and CRISPR-based gene editing [7]. As personalized gene therapies advance, the demand for an efficient, broadly applicable and reliable mRNA delivery platform grows. LNP formulations stand out by unique properties such as defined size, colloidal stability, low immunogenicity and the possibility of cell-specific delivery via surface functionalization. These properties are in parts the result of rational design approaches [8] and high-throughput screening of libraries of lipid-like compounds [9,10]. Current LNP formulations are composed of four lipid components: (i) ionizable lipid, (ii) helper lipids, e.g., DSPC (1,2-distearoyl-*sn*-glycero-3-phosphocholine), (iii) PEG (polyethylene glycol)-lipid, and (iv) cholesterol. It is understood that the favourable properties come about by optimal choice of these lipid components that ensure self-assembly into a well-defined core–shell architecture. Typically, PEG-lipid and helper lipids, such as DSPC and cholesterol, form a surface monolayer that stabilizes LNP size, while the ionizable lipid, cholesterol and nucleic acids reside in the core [2,11,12]. LNP manufacturing employs efficient condensation and encapsulation of negatively charged nucleic acid cargo with ionizable lipid at low pH via rapid microfluidic mixing, which promotes homogeneous self-assembly of lipid nanoparticles by fast solvent exchange [13]. Particle size and stability is adjusted via modification of core-lipids to shell-lipids ratio [12]. LNP formulations govern their ability to efficiently mediate cellular uptake via plasma proteins and subsequent release of nucleic acid to the cytosol. The LNPs were developed and first optimized for siRNA delivery [8,14,15]. Interestingly the same LNP formulations with only small adjustments proved also highly efficient for mRNA delivery [9,16]. In this review we will focus on mRNA-LNPs, but refer to siRNA-LNPs for comparison or in cases where corresponding data are not available for mRNA-LNPs. Over the past decade substantial progress has been made in optimizing LNP formulations turning both siRNA and mRNA LNP-based delivery into a manageable platform technology. However, quantitative pharmacokinetic modelling of LNP delivery and profound understanding of the delivery mechanism at the molecular level are still in their infancy.

The aim of the present review is to present a quantitative reaction kinetic framework of gene delivery and to collect kinetic rates for the various sub-steps leading to gene expression. We begin with an

* Corresponding author.
E-mail address: raedler@lmu.de (J.O. Rädler).

https://doi.org/10.1016/j.ejpb.2024.114222
Received 29 November 2023; Received in revised form 23 January 2024; Accepted 8 February 2024
Available online 20 February 2024

abstraction of nucleic acid delivery as a chain of transfer processes. Next, we introduce common reporter readouts and single-cell time lapse imaging. We then show that time courses of reporter gene expression reflect the reaction kinetics of a simple translation model. Single-cell expression exhibits distinct onset-times that indicate the delivery time as the period from LNP administration to mRNA release. We highlight factors that influence the uptake-rates and the existence of a window of opportunity in endosomal release. Experiments using multiple fluorescence markers or multiple mRNAs reveal distinct event-time correlations. We discuss codelivery of different mRNA reporter constructs and provide an outlook how timing can be modulated to achieve controlled gene expression.

2. Modelling LNP-based mRNA delivery

Quantitative modelling aspires to describe mRNA-LNP delivery as a sequence of discrete stochastic transfer processes [17–20]. As demonstrated in our earlier work [21] it is useful to dissect delivery in sub-steps as shown in Fig. 1. After administration of LNPs, rapid exchange of PEG-lipid and plasma proteins leads to the formation of a LNP protein corona. The protein corona enables LNPs to bind to the cell surface in a binding reaction followed by receptor mediated endocytosis. As discussed later in section 5 and 6, various pathways of endosomal uptake and endosomal processing exist. Most prominently, some endosomes are guided to undergo exocytosis, while other endosomes acidify due to the action of proton pumps and evolve into lysosomes. As a consequence, ionizable lipids become protonated and engender endosomal escape via LNP fusion with the endosomal membrane [9,20–23]. This crucial and still fairly unexplored step is subsumed in a single "escape" rate, k_L (Fig. 1). Subsequently mRNA is released from the remaining LNP shell into the cytosol. At this point, translation is initiated by ribosome binding and mRNA translation into protein, which in the case of a reporter protein like enhanced green fluorescent protein (eGFP) leads to a fluorescence readout (trajectories in Fig. 1). As detailed in section 4, eGFP fluorescence requires an additional chemical reaction known as maturation (with rate k_m). Each of the intracellular interstage products are continuously exposed to the risk of degradation. A further complication is the fact that many loaded endosomes differ in their number of LNPs as LNPs may enter endosomes either alone or as a cluster. The latter case has been addressed in multilevel modeling in reference [21]. For the sake of simplicity, we restrict ourselves to the linear model shown in Fig. 1. It is challenging, however, to reinforce the delivery cartoon by actual numbers. Only few of the kinetic rates have been measured. Furthermore most, if not all, parameters must be considered cell-type dependent. In order to provide data for quantitative modelling, single-cell time courses need to be recorded. Studying single cells allows us to get beyond the population average and to access cellular heterogeneity and subpopulations [18,24,25]. In more detail, single cell trajectories resolve rare events [26], event-time correlations [26,27], fluctuations and noise [28]. Fluctuations are seen in terms of cell-to-cell variability as well as intrinsic noise in expression trajectories, caused by stochastic nature of the underlying molecular processes. In any case, time-resolved microscopic observation is crucial to access LNP delivery and expression kinetics.

3. Reporter genes and time resolved microscopy

GFP provides the most convenient quantitative time-resolved measurement of protein expression [29]. GFP-reporters based on mRNA or plasmid vectors are widely used to signal the efficiency of nucleic acid transfer [30]. Moreover, the dynamics and spatial distribution of protein expression is readily observed in live-cell imaging. Variants of GFP exist that show enhanced or color shifted fluorescence allowing for monitoring protein expression of multiple genes in parallel [31]. Recently, more advanced reporters in terms of maturation speed, brightness and quantum yield became available such as mGreenLantern [32] or mScarlet [33]. In order to follow the fate of exogenous reporter genes during transfection, the nucleic acids can be labelled themselves using various nucleotide-bound cyanine dyes or dyes binding to 3′ UTRs of synthetic mRNAs [34,35]. Together with countless markers for live imaging of cell compartments and processes, high-resolution fluorescence imaging is a powerful method to unravel gene delivery pathways.

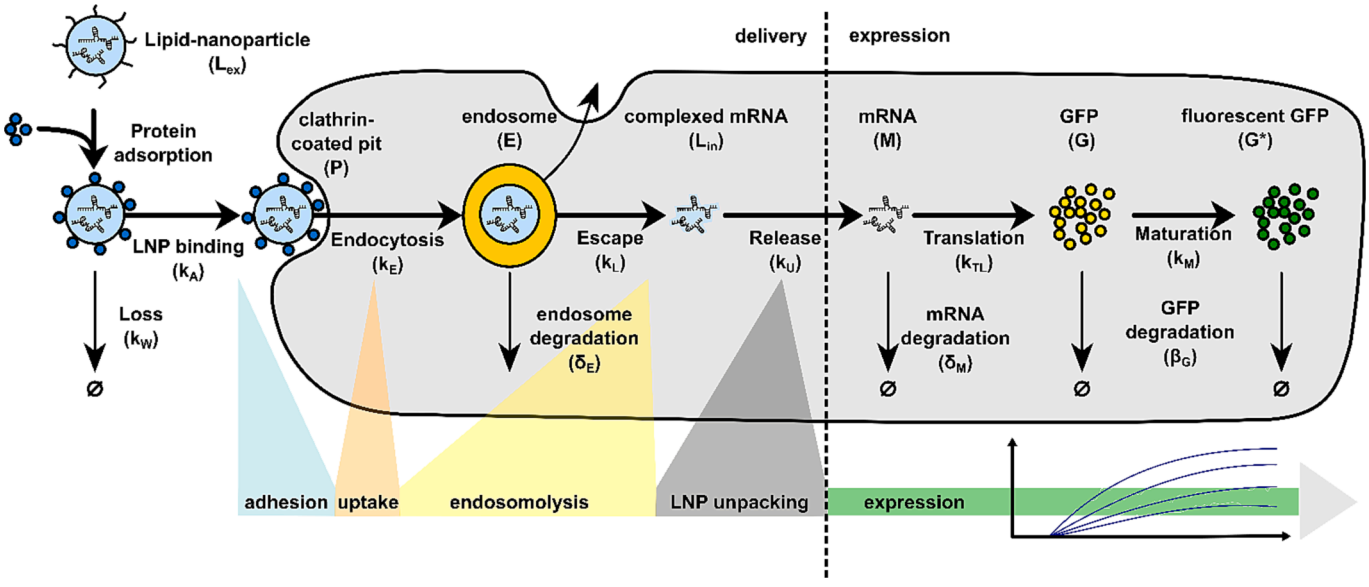

Fig. 1. Reaction pathway of mRNA-LNP delivery and expression: After incubation of LNPs to cell medium or blood serum PEG-lipid desorbs and protein adsorption decorates the LNP with proteins. The protein corona mediates LNP adhesion to the plasma membrane (blue timescale) and facilitates uptake (orange timescale). Subsequently, LNPs either undergo endosomal recycling (exocytosis), lysosomal degradation or endosomal escape (yellow timescale). Those endosomal escape events then result in cytosolic particles consisting of mRNA and residing lipids that can release their nucleic acid cargo (grey timescale). After those delivery steps, RNA is ready for cellular processing, here: mRNA translation for protein expression is depicted including steps of translation, protein maturation and potential degradation of both mRNA and protein species (green timescale). In case of reporter proteins, expression can be captured (inset with traces). Adapted from Ligon et al. [21] (© 2014 Ligon et al.). (For interpretation of the references to color in this figure legend, the reader is referred to the web version of this article.)

In particular, specific antibody labelling against clathrin or caveolin are available to follow endocytosis and intracellular processing of endosomes [34]. In addition to imaging of individual uptake and endosomal escape events, automated live-cell imaging is frequently employed to follow reporter gene expression over time. However, in order to obtain high-quality time resolved single-cell transfection data, platforms that provide identical local microenvironments are convenient. Micropatterned substrates enable us to collect high-quality fluorescence trajectories with sufficient statistics. Live-cell imaging on single cell arrays (LISCA) as described in Reiser, Krzysztoń, Murschhauser or Müller allows for high-throughput measurement of time resolved single-cell imaging and combines the above-mentioned techniques [26,36–38]. In short, arrays with cell-adhesive squares and a cell-repellent surrounding are produced and allow for cells to self-assemble to the single-cell pattern as depicted in Fig. 2a. Imaging under physiologic conditions over time (Fig. 2b) allows measurement of hundreds of single-cell fluorescence trajectories in parallel (Fig. 2c). This high statistic together with fine time-resolution allows modelling of gene expression as for example with a three-stage-maturation model described by Krzysztoń et al. (Fig. 2d) [37]. Further, this isolation of cells in defined adhesion sites results in standardized cell shape and hence area. However, it is to be noted that the lack of direct cell–cell contacts might result in adverse effects. Therefore, it is important to track cell division, survival rates and morphology as an indicator for vitality.

To quantify LNP uptake and release, real-time 3D particle tracking microscopy approaches [39] and analysis methods can help to obtain quantitative data over a large timespan. Tracking analysis led to great advancement in the field of virus-based vaccination [40,41]. In the case of LNPs, the molecular components, mRNA or lipids, can be labeled independently, revealing potentially different kinetics [42–44]. In recent studies, super resolution techniques like Stochastic Optical Reconstruction Microscopy (STORM), Stimulated Emission Depletion

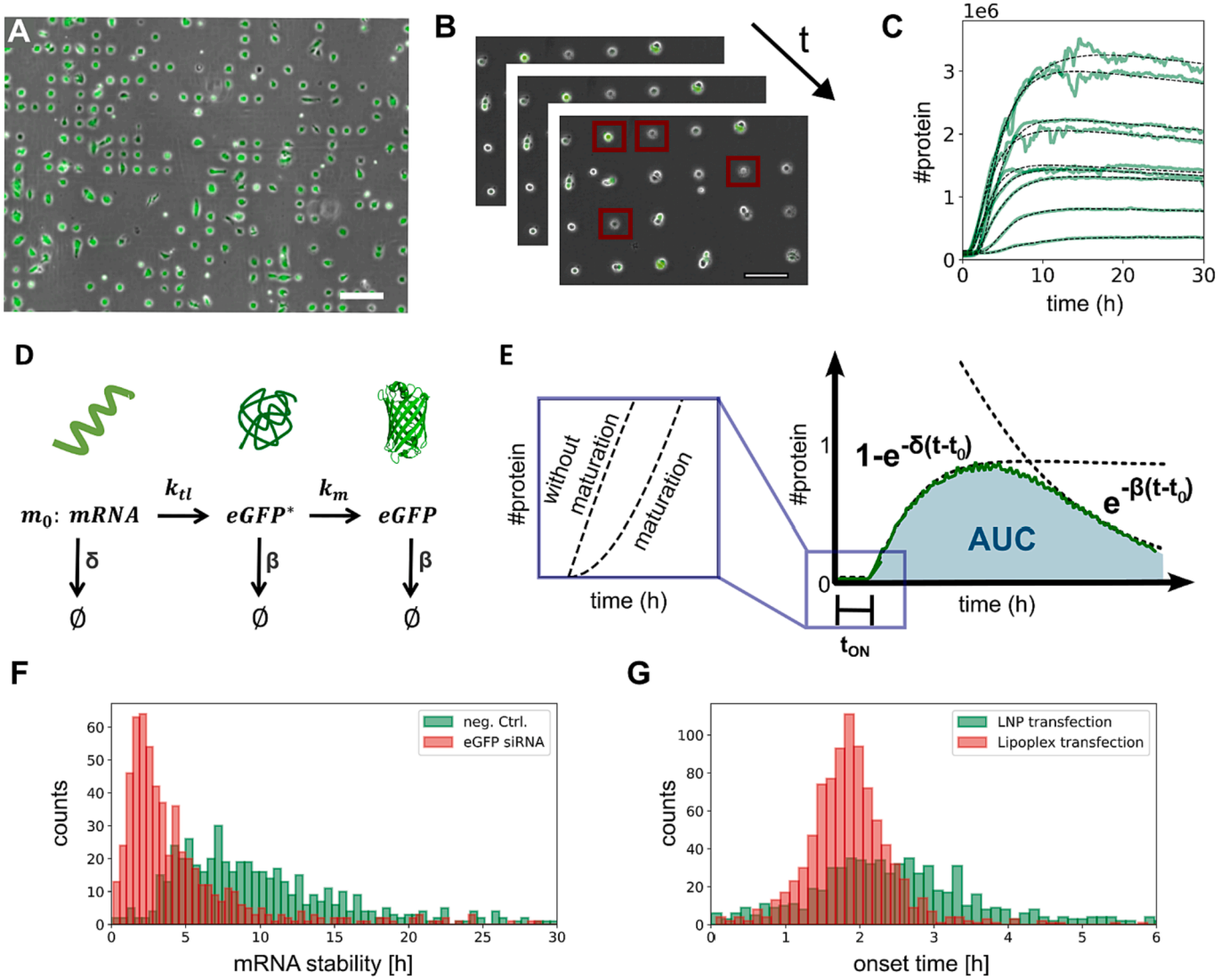

Fig. 2. Live Cell Imaging on Single Cell Arrays (LISCA) monitoring single cell reporter protein expression. (A) Micropatterned structures allowing for self-sorting of single cells on isolated adhesion sites. (B) Time-lapse movies under physiologic conditions generate (C) single cell fluorescence trajectories (green lines) which then can be fitted to quantitative models (black dashed lines). (D) translation-maturation model for GFP-mRNA expression according to Krzysztoń et al. [37]; adapted from Müller et al. [38]. (E) Predicted time course of GFP expression. Protein production and protein degradation are separately depicted by exponential functions with mRNA degradation rate δ and protein degradation b as respectively. The total transient protein expression is shown as shaded region (AUC) and calculated from the fit as described in section 3. Correct determination of the expression onset-time distribution requires consideration of the GFP maturation step. (F) Distributions of mRNA stabilities with and without siRNA (Dharmacon, GFP Duplex I siRNA) mediated knockdown. (G) Distributions of onset-times from fits of hundreds of trajectories shows faster transfection mediated via cationic lipoplexes compared to LNPs. (For interpretation of the references to color in this figure legend, the reader is referred to the web version of this article.)

Microscopy (STED) or the Structured Illumination Microscopy (SIM) are used to observe the trajectory of endosomes inside eucaryotic cells [45], the release of siRNA loaded nanovectors [46], the shape of nanocarriers [47] and the clustering of LNPs inside the early endosome [48]. As the release mechanism is little understood, it is beneficial to record the endosomal trajectories simultaneously with information about the microenvironment, a feature that most current imaging techniques lack [49].

To enhance our understanding of endosomal release kinetics and trajectories, more sophisticated imaging methodologies are needed. Among these, fluorescence lifetime imaging microscopy (FLIM) stands out as a useful technique. Fluorescence lifetime, the average time a fluorescent molecule spends in its excited state, is highly sensitive to the fluorophore's immediate biochemical environment. Variations in photophysical properties, such as those induced by fluctuations in pH-Value, temperature, or the solvent polarity, are detectable through changes in fluorescence lifetime [50,51]. This sensitivity exceeds the capabilities of traditional intensity-based microscopy techniques, which is constrained by morphological details. The specificity of this parameter to environmental factors has pushed extensive research into creating specialized fluorophores. Such probes are engineered to respond to changes within microenvironments, like subcellular pH levels within cytosolic regions of endosomes and lysosomes [52]. Fluorescence lifetime measurements can also be used to incorporate techniques like the förster resonance energy transfer (FRET) [53–55]. FRET's sensitivity to subnanometer-scale changes allows for detailed examination of lipid membrane dynamics [56] crucial to endosomal release, offering precise insights into the details of cellular trafficking processes. By incorporating fluorescence lifetime measurements simultaneously with other techniques, a richer understanding of the multifaceted mechanisms of the endosomal release can be achieved.

4. Mathematical model of mRNA-LNP mediated protein expression

When mRNA is released into the cytosol, protein expression is turned on (green area in Fig. 1). In a coarse-grained view, mRNA translation is described as a biochemical reaction and a corresponding mathematical model is readily set up. As described in the original work by Leonhardt in 2014 [18] the rate of protein (P) production in an individual cell is given by

$$\frac{d}{dt}P = k_{TL}\cdot m - \beta\cdot P \tag{1}$$

where k_{TL} is the translation rate, m the number of accessible mRNA molecules in the cytosol and β the degradation rate of protein. As mRNA has a finite life-time the concurrent decay of mRNA is described by

$$\frac{d}{dt}mRNA = -\delta\cdot m \tag{2}$$

where δ denotes the degradation rate of mRNA. Eq. (1) and Eq. (2) can be solved yielding the following analytical expression for the time course of the number of proteins

$$P(t) = \frac{m_0\cdot k_{TL}}{\delta-\beta}\cdot\left(1-e^{-(\delta-\beta)(t-t_0)}\right)\cdot e^{-\beta(t-t_0)} \tag{3}$$

where m_0 denotes the number of mRNA molecules that are in an idealized view instantly released at a given point in time, t_0. Eq. (3) provides a prediction for the time course of number of proteins in a single cell. In the case of eGFP reporter genes, P(t) is proportional to the total eGFP fluorescence emanating from a single cell (Fig. 2c). Fig. 2d explicates the characteristic features of the expression dynamics resulting from Eq. (3). At time point t_0, which we term the onset-time, fluorescence sets in and shows an initial linear increase with slope m_0k_{tl}. The onset-time hence is an idealized time point when m_0 mRNA molecules are thought to be concurrently set free and bound by ribosomes for consecutive production of protein. The rate of fluorescence increase exponentially slows down as mRNA is degraded. As indicated by the dashed line in Fig. 2e, the protein level would saturate at a constant value, if proteins were stable ($\beta = 0$). With finite protein stability, eGFP fluorescence reaches a maximum and approaches a regime dominated by exponential decay at long time scales. We recall the protein half-life, i.e., the time when half of the initial protein is left over, is given by $\tau_{GFP} = \ln(2)/\beta$. Likewise, the half-life of mRNA is defined as $\tau_{mRNA} = \ln(2)/\delta$. Note that τ_{mRNA} represents the functional life-time of mRNA, i.e., the time until mRNA translation ends, which is different from molecular degradation or the time until mRNA can no longer be detected e.g., via FISH probes. As a rule of thumb, τ_{mRNA} is equal to the time the expression needs to reach half-maximum of the expression level and τ_{GFP} the time scale of expression decay. Without loss of generality, we can assume that the degradation rate of mRNA is larger than the degradation rate of eGFP protein, $\delta > \beta$. This is confirmed by measuring the protein degradation in an independent experiment. To this end, after some initial expression, the drug cycloheximide is added, which immediately inhibits translation. In this case, the single exponential fluorescence decay is solely determined by protein degradation [37].

Due to the finite life-time of both mRNA and protein, the expression of protein is transient. In this context the measured "area under the curve" (AUC) is generally used to describe the overall pharmaceutical protein availability. We obtain the theoretical AUC of the expression model by integration of Eq. (3)

$$AUC = (ln2)^2\cdot m_0\cdot k_{TL}\cdot\tau_{mRNA}\cdot\tau_{EGFP} \tag{4}$$

Eq. (4) is astoundingly insightful. It states that the AUC, and hence pharmaceutical efficacy, is equally dependent on four factors, the number of mRNA molecules delivered, the translation rate, the mRNA life-time and the protein life-time. Each of these factors is equally important in order to maximize efficiency. In fact, single-cell time courses can be used to screen for optimal rate constants such as increased mRNA life-time using stabilizing UTR sequences as demonstrated by Ferizi et al. [57]. Fitting experimental fluorescence time courses yields single-cell values for four parameters: the two degradation rates (β and δ), the expression rate m_0k_{tl} and the onset-time t_0. Note the expression rate, i.e., the speed of protein production, is determined by both the initial number of mRNA molecules and the translation rate, and it is not possible to separate these two factors from the analysis of the fluorescence time courses alone. Fig. 2f shows a two-color histogram of single-cell eGFP-mRNA stabilities. The histogram reflects the effect of decreasing mRNA stability in the presence of targeting siRNA (Dharmacon, GFP Duplex I siRNA) (Fig. 2g). Another meaningful histogram is the distribution of expression onset-times dependent on the carrier as shown in Fig. 2f. In this case, another subtle effect needs to be considered. GFP fluorescence appears somewhat delayed after completion of protein translation. This is due to the fact that GFP undergoes an additional autocatalytic chemical reaction, known as maturation, that leads to the formation of the cyclic chromophore inside the protein barrel [30]. Including maturation into the system of chemical rate equations (see Fig. 2d) results in time course P(t) with slightly delayed onset as shown in the inset of Fig. 2e. In the work of Krzyszton *et al.* we showed that inclusion of maturation improves the overall quality of best fits of the mathematical model to experimental time courses [37]. Note that including protein maturation in the mathematical description of mRNA translation fits experimental fluorescence time courses very well (dashed line in Fig. 2c). However, deviations from Eq. (3) can be seen at very high expression levels, when the expression burden on the organism is high [58]. Interestingly, the experimental single cell time courses are well described by a model which assumes that all mRNA is released at a particular time, t_0. This fact supports the notion that, most likely, all mRNAs are released from a few endosomal fusion events occurring in a narrow time window. Moreover, in the case of relatively stable mRNAs

and proteins the heterogeneity in transfection onset times is less prominent and ensemble average data exhibit a similar time course as described by Eq. (3). For example, time resolved plate reader data could be fitted with the same model yielding estimates of average protein lifetime and translation rate. However, single cell analysis clearly is the preferred access to expression kinetics as it not only yields the full distribution of rates across the population, but also allows us to correlate kinetic rates and event times as discussed below. The question, what causes cellular heterogeneity in expression onset suggests itself. As shown in Fig. 1, the transfer of LNPs into the cellular cytosol is dissected into at least three stochastic processes, namely uptake, endosomal fusion and mRNA release and will be discussed in the following sections.

5. Endosomal uptake

RNA loaded LNPs are internalized by cells via endocytosis [59]. Various endocytic pathways can be classified: the receptor-mediated caveolin or clathrin-mediated endocytosis (CME) as well as the receptor-independent micropinocytosis and phagocytosis [60–62]. The intracellular fate and hence the cytosolic delivery efficiency of internalized particles is determined by the path of entry [63,64]. The uptake path is further dependent on the particle characteristics as well as cell type [65]. The dominant path of entry is the receptor-mediated endocytosis [23]. Specifically, CME uptake requires receptor binding that is mediated via the passively formed protein corona consisting of ApoE targeting low-density lipoprotein (LDLR) interaction [66], high-density lipoprotein (HDL) coating as recently described by Liu [67], Lipoprotein-D coating (Fig. 3a) [68] or tumor cell type specific coating with albumin [69]. LNP uptake in particular is mediated by PEG-lipid dissociation and concomitant protein adsorption [70]. Enhanced uptake via protein corona is a frequently occurring phenomenon on nanoparticle-cell interactions. In case of positively charged polyplexes, the negatively charged serum proteins assemble around the polyplex and facilitate uptake via CME [71]. In applications where highly specific targeting is required, uptake can be promoted by addition of targeting ligands to the LNP shell [66] or adapt lipid composition to target different tissues [72]. For example, T-cell targeting LNPs have recently reached clinical studies for next generation CAR-T cell therapies [6,73,74].

Time estimates for how long uptake after receptor binding takes, vary in the literature. Table 1 provides an overview of uptake time data from selected works varying in the proposed mechanism as well as type of studied particle and cargo. In general, literature proposes uptake times for mRNA LNPs from several minutes [18,69,75] to several hours [42,76,77]. Based on fluorescent labelling and confocal microscopy Gilleron *et al.* reported a timing for the uptake of siRNA LNPs ranging from 0.5 to 1.5 h for CME and 2–6 h in case of micropinocytosis [60]. For comparison, the well-studied viral uptake in case of CME is in the range of seconds (e.g. AAV-2 s) to minutes (e.g. HIV-1 s) [78]. Studies using smFISH showed a high uptake rate during the first 4 h after transfection and subsequent slow-down of uptake [42]. Advanced imaging setups as two-photon microscopy (Fig. 3b) or single particle tracking (SPT) allows to distinguish between random movement and active transport and showed that uptake can be distinguished in 3 phases that strongly depend on carrier and cell type [44,64]. It is generally believed that uptake and hence efficiency is dependent on nanoparticle composition [79] and size. Large particles in the μm-range enter the cell via micropinocytosis [80], for particles smaller than 500 nm the caveolae-dependent pathways appeared to be dominant in accordance with the finding that CME has an upper size limit of 200 nm [81]. Theoretical considerations lead to predictions of an optimal size for entry of 30 to 60 nm [82], which is in accordance with theoretical findings for polymer nanoparticles [83], whereas the maximal efficiency for mRNA-LNP based vaccines was found for 100 nm sized particles

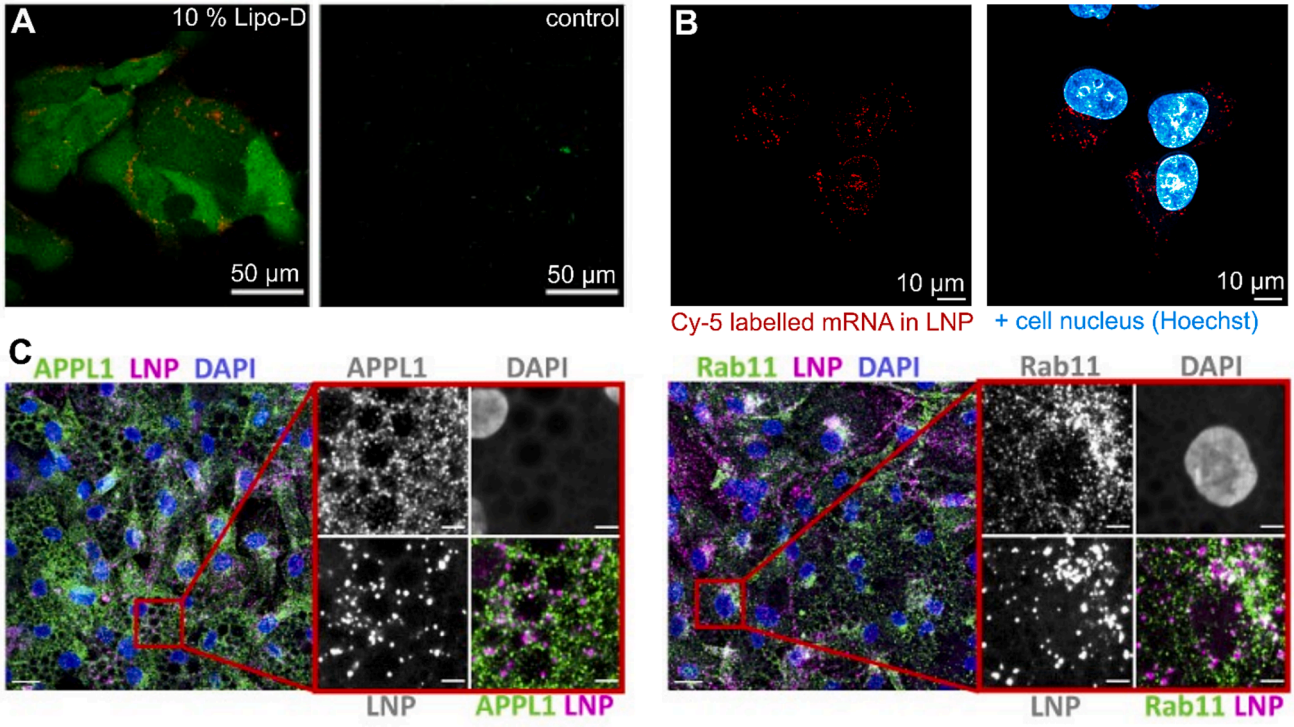

Fig. 3. Imaging of kinetics of LNP-RNA uptake and release: (A) HuH7 expressing eGFP upon transfection with LNPs encapsulating Cy5-eGFP-mRNA. LNPs were pre-incubated with or without 10 % Lipo-D protein. Cells were fixed and imaged with confocal microscopy [68] (© 2022 Aliakbarinodehi et al.). (B) Two-photon microscopy images recorded with a 60x water immersion objective. An ultrashort pulsed laser at 80 MHz with wavelengths of 1034 nm 780 nm was used as excitation source. Image analysis was performed using Fiji and Huygens software (unpublished data). (C) Human primary adipocytes after incubation with LNPs encapsulating fluorescently labeled mRNA. After 2 h cells were fixed and antibody labeled for endosomal markers (shown here: early endosomal marker APPL1 and late endosomal marker Rab11). Reprinted with permission from Ref. [79] (© 2021 Paramasivam et al).

Table 1
List of uptake times and corresponding uptake mechanism.

First Author	Year	Estimated Time	Proposed mechanism	Type of particle	Method
Dahlman [76]	2017	Maximum after 2 h	n/a		DNA barcodes *in vivo*
Miao [69]	2020	15 min	CME or micropinocytosis		Fluorescence microscopy
Miao [69]	2020	15 min	CME or micropinocytosis		Fluorescence microscopy
Patel [42]	2020	Within 4 h	n/a		3D Single particle tracking
Gallud [75]	2021	17 min (+2h if no serum incubation)	PEG shedding + LDLR receptor dependent	**LNP + mRNA**	Single NP imaging, NMR diffusometry, SANS, Proteomics, DLS
Munson [77]	2021	4–10 h	n/a		Live-cell imaging
Paramasivam [79]	2022	2–24 h (i-lipid dependent)	n/a		Super resolution microscopy
Liu [67]	2023	n/a	HDLR dependent		Multiomics
Aknic [66]	2010	n/a	LDLR dependent		Automated spinning disc confocal microscopy (fixed or live cells)
Gilleron [60]	2013	1.5 h	CME	**LNP + siRNA**	Blocking or knock out of respective components, Colocalization experiments of LNP and Rab5, EM
Hunter [103]	2023	n/a	Receptor mediated endocytosis	70 nm LNP + siRNA	Confocal microscopy + machine learning
		2–6 h	Micropinocytosis	larger LNP + siRNA	
Leonhardt [18]	2014	10–30 min	n/a	Lipoplex + DNA	LISCA
Rensen [131]	2001	n/a	GalNAc/ASGPR dependent uptake	Liposomes	Radiactive labelling and live-cell fluorescence microscopy

[84]. Interestingly, a CME endosome is only about 100 nm in diameter and hence has limited LNP capacity [62]. A recent study also showed that LNP shape matters, observing a higher uptake for star-shaped LNPs compared to round LNPs [85].

6. Endosomal fusion and mRNA release

Next, we discuss the timing of endosomal escape, considered as the bottleneck in LNP-based delivery of mRNA [86]. Following receptor-mediated uptake, LNPs are trapped in early endosomes with an internal pH ranging from 5.5 to 6.5 followed by maturation into late acidic endosomes with a pH of 5–5.5 [77,87,88]. Acidification of endosomes is likely to be crucial for fusion of LNPs with the endosomal membrane [89]. LNPs that do not escape the endosome at this stage are degraded or exocytosed [86,90,91]. Degradation through lysosomal fusion enriches the endosome with degrading enzymes while Rab-mediated signaling transports endosomes towards the plasma membrane and enables fusion for exocytosis. In fact, the majority of LNPs undergo one of the later pathways and hence do not deliver mRNA to the cytosol [59]. Escape efficiency is generally defined in terms of percentage of trapped LNPs that escape from the endosome. Some measurements of escape efficiencies are listed in Table 2 ranging from 2 % [60] to 3.5 % [92] for siRNA-LNPs and for mRNA LNPs from 1 % [93] up to 15 % with Moderna's own ionizable lipid 5 [94], similar to theoretical calculations predicting 14 % escape [95].

The timing of endosomal fusion is a key factor for delivery efficiency. It appears that only within a narrow window of opportunity the conditions allow LNPs to escape through endosomal fusion [86]. A correlation between fast endosomal trafficking and expression efficiency was described [88]. Different timescales were reported (Table 3), ranging from 0 to 1 h in case of small endosomes [79] or more general, 5 to 15 min [96] and up to 4 h [88]. Gilleron et al. described a gradual increase of siRNA-LNPs in the endosome within the first 4 h after uptake with a maximum co-localization of siRNA-LNPs in the endosome after 1 h [60].

Since the discovery of cationic lipid-mediated nucleic acid delivery, an extensive search for factors affecting endosomal escape efficiencies has been conducted. In early studies on DNA-lipoplexes it was demonstrated that cationic lipids complex into liquid crystalline nucleic acid–lipid complexes [97] and that inverse hexagonal mesophases showed higher delivery efficiency than lamellar phases [98]. LNPs made from cationic ionizable lipid likewise condense nucleic acid at low pH during the microfluidic mixing process. LNPs exhibit electron-dense core structures in cryo-TEM with a wide range of polymorphism. In the work by Arteta *et al.* using X-ray scattering it was shown that in the case of DLin-MC3-DMA the core phase consists of an inverse hexagonal phase [12]. Other LNP forming lipids exhibit cubic phases [99]. Recent X-ray studies revealed that the LNP core phase undergoes structural changes as a function of pH [100–102]. It is hypothesized that acidification-induced structure evolution inside LNPs leads to endosomal destabilization. pH driven lipid head group charge as well as release of elastic membrane energy favor membrane fusion. Local pH change as a prerequisite of LNP fusion and acidification of the endosome is a rate limiting factor in

Table 2
List of estimated times of endosomal release.

First Author	Year	Estimated Time	Type of Nanoparticle	Method
Miao	2020	15–30 min	LNP + mRNA	Confocal microscopy, qPCR
Gallud	2021	12 min	LNP + mRNA	
Alakbarinodehi	2022	5–15 min	LNP + mRNA	Live-cell TIRF, supported membranes
Kirschmann	2017	5 h	Lipoplex + mRNA	Spinning disc confocal microscopy
Gilleron	2013	Up to 6 h	LNP + siRNA	Quantitative light and electron microscopy
Wittrup	2015	5–10 min	LNP + siRNA	Gal9 recruitment,
		5–15 min	Lipoplex + siRNA	Fluorescence imaging in two modi (long and short exposure)
Wrobel&Collins	1995	1–2 min	Liposomes + DNA	Fluorescence microscopy
Sonawane	2003	30–75 min	PEI + DNA	Cl- sensing fluorescenct probes

Table 3
Endosomal release efficiencies in percent of LNPs that are released into the cytosol from the total taken up.

First Author	Year	Estimated Efficiency	Type of Nanoparticle	Method
Sabnis	2018	15 %	LNP + mRNA	Fluorescence microscopy, Moderna lipid
Maugeri	2019	1 %	LNP + mRNA	EV extraction, qPCR, UPLC
Gilleron	2013	1–2 %	LNP + siRNA	Quantitative light and electron microscopy
Wittrup	2015	3.5 %	LNP + siRNA	Gal9 recruitment, Fluorescence imaging in two modi (long and short exposure)

endosomal release. Endosomal escape is favored at late stages when the LNP reaches the cytosolic area around the nucleus [103] and their active transport seems to be higher for small endocytosed particles [71]. Also, the number of LNPs in the endosome is relevant as several particles per endosome were discussed to block required acidification possibly due to the buffering effect of the ionizable lipid [68,79]. Furthermore, the optimal pH for endosomal escape is lowered by the protein corona, dependent on its composition [68]. Whereas Paramasivam et al. [79] described an independency of the type of ionizable lipid and timing, many others tackled the influence of the ionizable lipid on escape efficiency [94,104]. Cholesterol and analogues enhance membrane fusion [42] and stabilize high curvature regions [105]. PEG type and ratio change not only the expression level but also the expression kinetics [76,106]. Release of mRNA into the cytosol requires phase separation and membrane fusion. Therefore, the protein corona needs to be removed at least partially [107]. Apart from the lipid composition, also the type of RNA cargo might interfere with endosomal escape. Endosomal escape differs for mRNA compared to siRNA: The amount of co-localization of siRNA-LNPs with small endosomes reduces after 1 h whereas the amount of mRNA in large endosomes saturates after 1 h with no decrease until 2 h after uptake [60,79]. This leads to the general question if there is a relation between uptake pathway and release efficiency, respectively degradation. It was observed that there are at least two different types of endosomes (e.g. RAb11 positive vs. ACU22 positive as depicted in Fig. 3c) with different escape probabilities [79]. Maugeri et al showed that the endocytosis and the packaging into extracellular vesicles (EVs) for secretion are linked [93]. Furthermore, an influence of endosomal size and endosomal escape was described [108] and endosomal size is dependent on the endocytic pathways [62]. Peetla *et al.* discussed that the interaction of LNPs with artificial plasma and endosomal membranes differs [109]. Reiser *et al.* studied uptake kinetics and transfection efficiency for different cell media and found a concerted population correlation dependent on serum concentration (see also Fig. 4a) [110]. Similarly, Aliakbarinodehi found that the protein corona enhances cellular uptake and, at the same time, shifts the endosomal escape towards lower pHs and therefore to later timepoints and lower probabilities [68]. These opposing trends were also described by Miao *et al.* [69]. Nevertheless, it is to be noted that maximum protein expression does not necessarily increase in a linear manner with enhanced endosomal escape as cellular resources are limited but a more efficiently escaping drug might lower dose requirements [77,79]. Further, the linear delivery model as described in Fig. 1 includes a step where the mRNA escapes from residual lipids to become available for the translation machinery. To access this step, mRNA can be labelled and tracked over time to observe an increase of fluorescence upon unpacking. Simultaneous tracking of reporter protein expression allows to measure the time window between release and start of protein expression as shown in Fig. 4b [102].

7. Codelivery of different nucleic acid agents

Codelivery of multiple distinct elements is an increasingly relevant necessity in advanced rational design gene therapy. For example, codelivery of mRNA and siRNA allows for more effective targeting of cancer cells by simultaneous knockdown of oncogenes and overexpression of tumor suppressor genes [111]. Likewise mRNA/siRNA codelivery improves CAR-T cell engineering by expressing chimeric antigen receptor (CAR) mRNA together with siRNA knockdown of the programmed cell death protein (PD-1) in primary human T cells [112]. Also the expression of a pDNA mediated transgene was shown to be prolonged by simultaneous codelivery of anti- inflammatory siRNAs [113]. The relevance of nucleic acid codelivery was recognized at the latest with the rise of CRISPR/Cas based therapies, which typically require Cas9 protein and single guide RNA (sgRNA). These components are commonly delivered via adeno-associated viruses (AAVs) [114] but face limitations due to the limited packing size of AAVs [115] and redosing challenges [116]. LNP-based codelivery allows for selectable combinations of synthetic Cas-mRNA and sgRNA [117–120] or Cas RNP, sgRNA plus donor DNA [121]. In all these examples, codelivery of different nucleic acid elements is expected to unfold a synergistic effect. To this end, however, it is important to ensure synchronized release kinetics and action. Time-resolved single-cell studies employing two-color fluorescence enable to scrutinize the timing in codelivery [122].

In general, LNP-based codelivery of two RNA species can be achieved by two strikingly unlike mixing protocols: Each delivery agent can be encapsulated independently prior to combined administration (post-mixing protocol) or all components are jointly encapsulated in mixed nanoparticles (pre-mixing protocol). The first bears the advantage that each component can be encapsulated in its ideal vehicle and dosing can, if required, happen in cascades [37]. Yet, there is a remarkable difference between pre-mixing and post-mixing codelivery efficiency. In case of codelivery of two different GFP reporter genes, both for pDNA-lipoplex [95,122] as well as mRNA-LNP delivery [95], the percentage of cells that express both genes is higher for pre-mixing compared to

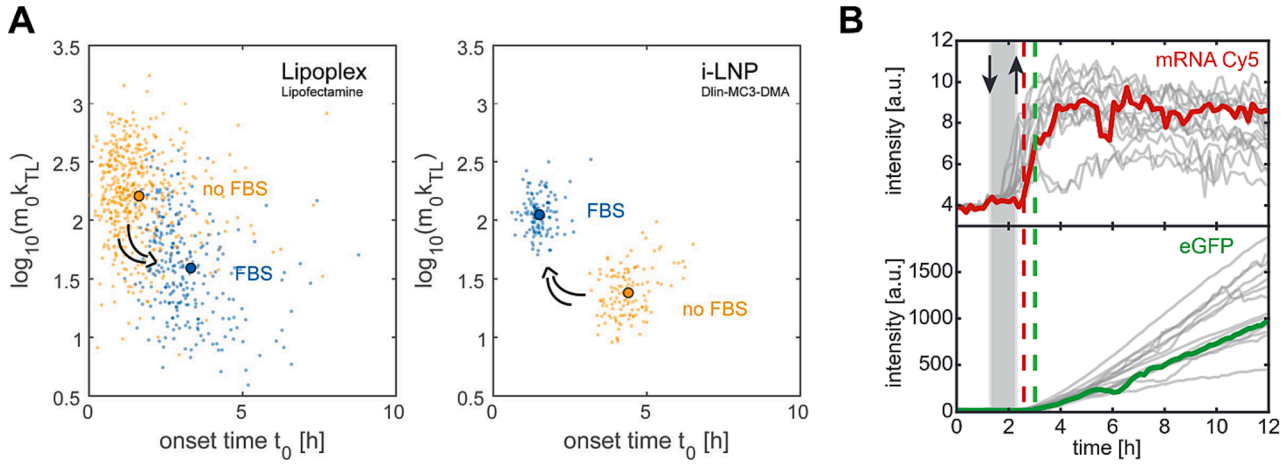

Fig. 4. Measuring rates of uptake and unpacking (A) Correlation plot of single cell onset times versus expression rates m_0k_{tl} of LNP-mediated and lipoplex mediated GFP expression measured independently with LISCA in presence and absence of serum. Reprinted with permission from Ref. [110] (© 2019 Reiser et al.). (B) Fluorescence trajectories of Cy5-labelled mRNA and eGFP protein expression signal during MC3-LNP mediated transfection. Time difference indicates a distinct time difference between endosomal release and mRNA unpacking. Grey bar marks the incubation period, red lines the respective onsets. Reprinted with permission from Ref. [102] (© 2023 National Academy of Science). (For interpretation of the references to color in this figure legend, the reader is referred to the web version of this article.)

post-mixing. Fig. 5a,b provides an example from Ref. [95] that shows the red-green fluorescence co-expression outcome as a function of the molar ratios of red/green encoding mRNAs in single RNA LNPs (S_R and S_G) compared to mingled LNPs (M_{RG}). In the regime of equimolar delivery post-mixing, i.e., delivery of either red or green encoding LNPs the percentage of co-expression is lower as seen by the heterogeneous distribution of cells that express only red or green. The experimental red/green likelihoods are quantitatively explained by stochastic mRNA-LNP uptake in the limit of small success rates of endosomal escape LNPs [95,122]. In recent work also the kinetics of co-expression were studied with the interesting observation, that differences in red/green onset-timing exist despite the fact that red and green encoding mRNAs were delivered in pre-mixed LNPs [37]. Fig. 5c shows exemplary single-cell fluorescence time courses for eGFP and CayRFP respectively, with clearly time shifted onsets, which also manifests in the onset-time correlation plot showing the entire population of single data (Fig. 5d). Possible reasons for this yet unexplained mRNA specific expression onset shift might be different release times, i.e., mRNA unpacking kinetics after endosomal release or different translation timing. While the former might be possible due to different secondary structure of the two distinct mRNA constructs, the latter could be caused by different untranslated region (UTR) and initiation site design. Also, base modification introduced to reduce the immunogenicity of mRNA were shown to influence uptake of LNPs in a tissue specific manner [123] and therefore needs to be considered in codelivery.

The issue of delayed expression gains further complexity as more than one type of nucleic acid species is encapsulated. It was discovered previously that mRNA and siRNA form different internal structures within an LNP [27] which has the potential to affect release and therefore expression timing. siRNA was found to be complexed into aqueous pockets by the phospholipids in the LNP. This leads to several questions regarding the molar ratio in codelivery of two species that have different physico-chemical properties: Are premixed LNPs homogenous in composition and if so, does the LNP nucleic acid content mirror the molar ratio that was set during LNP preparation? How many nucleic acid molecules are exactly contained in a single LNP? Based on SAXS structural data the number of mRNAs in LNPs varies as a function of size ranging from 10 molecules in LNPs of 50 nm diameter up to 200 molecules in LNPs with 140 nm [12,95]. Interestingly the number of functional mRNA molecules derived from statistical analysis of red/green fluorescence in codelivery was found to be 27 for 300 nm sized lipoplexes [95,122].For siRNA/mRNA no equivalent studies exist but an enhanced overall siRNA-mediated knockdown was reported for siRNA when codelivered with mRNA [111]. Little is known about discriminating or synergetic effects in endosomal escape and subsequent depacking in siRNA/mRNA codelivery. Furthermore, each species has

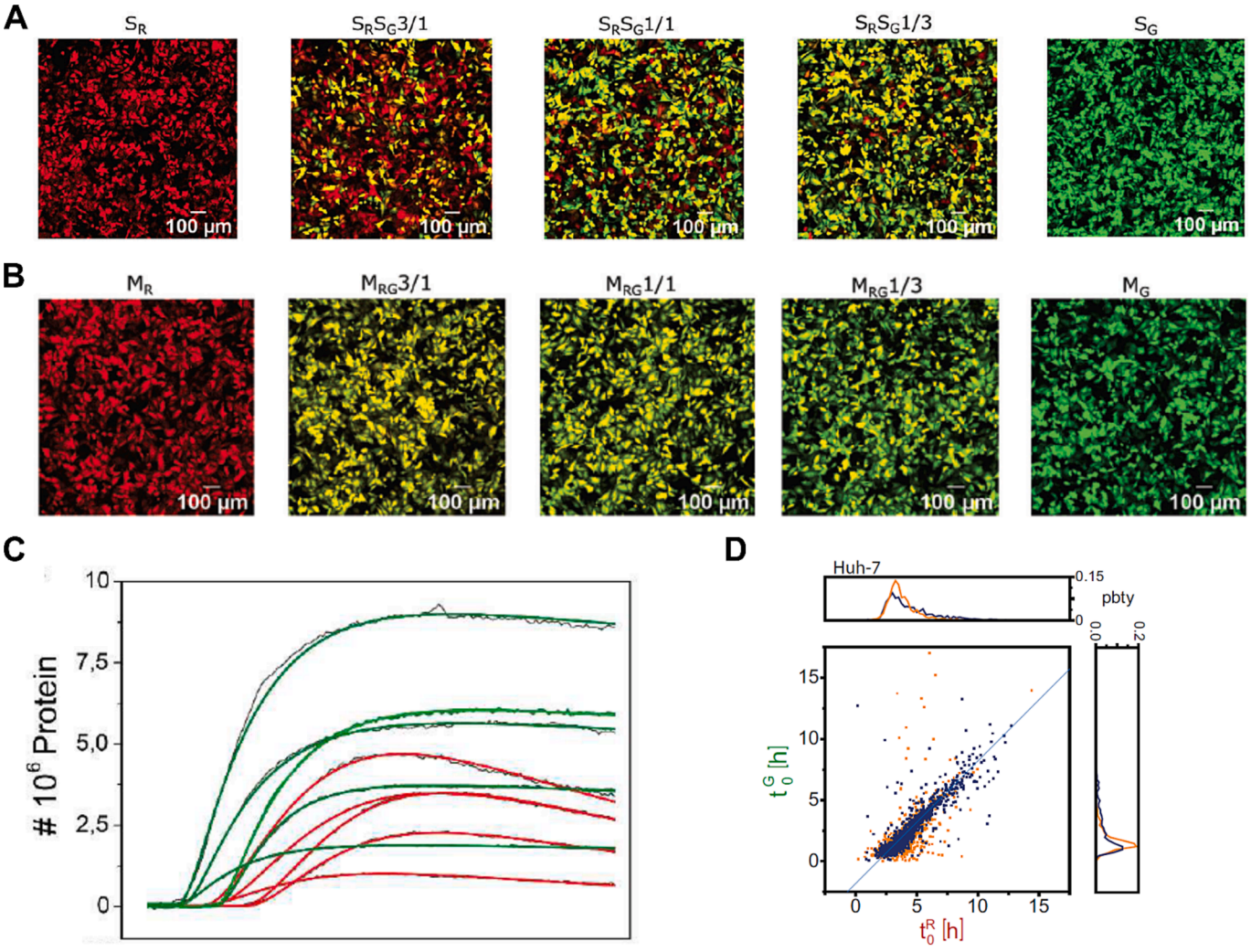

Fig. 5. Co-Delivery of RNA. (A) Co-delivery of LNPs with different ratios of mCherry-mRNA to GFP-mRNA encapsulated in single lipoplexes (S_{RG}) (B) different ratios of mRNA encapsulated in mingled lipoplexes (M_{RG}). (C) Single cell traces of HuH7 cells transfected with co-encapsulated RFP-mRNA and GFP-mRNA show shifted onset of protein expression. (D) correlation plot of GFP vs. RFP onset time distribution. (A)&(B) reprinted with permission from Ref. [95] (© 2021 Zhang et al.), (C)&(D) reprinted with permission from Ref. [37] (© 2019 Krzysztoń et al.).

different dynamics that need to be taken into account. Protein expression upon mRNA delivery is dependent on translation initiation, translational speed and protein maturation which is of special interest if the readout is a fluorescence reporter protein [37]. In contrast, siRNA needs to be spliced by the Ago Protein, assemble the RNA-induced silencing complex (RISC) and trigger mRNA degradation.

In case of CRISPR/Cas gene editing the cargo conveyed by the delivery vehicles consists of Cas protein and guide RNA (gRNA). Three discernible cargo options can be chosen: pDNA, mRNA, and ribonucleoproteins (RNPs). pDNA entails the delivery of genetic material in plasmid form, necessitating its entry into the nucleus for subsequent expression. This approach offers stability and prolonged expression but is associated with increased off-target effects and challenges in controlling the number of plasmids per cell [124]. Transfection can be done with one plasmid encoding for both Cas and gRNA, which ensures co-expression, simplifying the process but requiring cloning in large plasmids for each gRNA and/or Cas protein. However transfecting Cas and gRNA on separate plasmids allows independent control but necessitates co-transfection, introducing additional complexities [122]. In contrast to pDNA, mRNA is directly translated upon delivery, bypassing the nuclear entry step. This method possibly enables faster edits. However, it suffers from lower stability and delivery limitations due to the size of the Cas mRNA [125]. Timing differences were for example observed in Cas9 expression maxima that were measured after 36 h [118] whereas expression maxima for eGFP or CayRFP were found to peak after 15 to 20 h [37]. A difference in mRNA length (approx. 1000 nt for eGFP and CayRFP and 4500 nt for Cas9) is known but which part of the expression kinetics this impacts in which way is unknown up to date. Further to be mentioned is the timescale of sgRNA whose efficiency is described with the whole CRISPR process and is therefore ultimately extended. Apart from the different timescales of the various processes, also the different stabilities of for example mRNA and sgRNA relevant for CRISPR systems need to be taken into account [118]. RNPs, on the other hand, are preassembled complexes consisting of the Cas protein and gRNA. This structure renders them immediately functional within the cellular environment, allowing for prompt and precise genome editing actions. Challenges here include the protein extraction [125] and the missing continued production of Cas and gRNA [126]. Further considerations should also be given to the possibility of mixing cargo and delivery methods, i.e., Cas pDNA and later transfected gRNA as mRNA, which could offer timed advantages, but also strain cells more with multiple transfection periods [124,127]. Selecting the optimal CRISPR delivery method is crucial for achieving efficient and accurate genome editing. The best choice of a specific cargo delivery strategy with regards to stability, control, and efficiency is still a matter of current research. Rational design approaches will have to take the delivery kinetics into account.

8. Summary and perspective

In this paper we reviewed the kinetics of LNP mediated delivery of RNA. Uptake, escape and RNA release of LNPs can be effectively modeled as a series of discrete stochastic transfer processes, wherein each step can be described by distinct rates. We discussed those rates that have been measured in isolated studies using advanced time resolved microscopy techniques. In particular, the time course of mRNA mediated reporter gene expression is well documented in single-cell time-lapse studies and found to be in full agreement with reaction kinetics of translation, GFP maturation and associated degradation rates of mRNA and protein. Kinetic modelling contributed a substantial progress in our mechanistic understanding and consequently predictive power. Quantification of underlying rates and timescales is the basis for systematic screening approaches that aim to improve transfection and transient expression at every level of the multistep process. Time courses determine AUCs and have tangible implications in clinical applications [128]. The kinetic model of protein expression is universal and hence the analytic expression is widely useful. For example, in the work of Sabnis et al [94] the level of secreted protein hEPO and IGG protein was measured over days showing a qualitatively similar asymmetric time course as described in our model albeit with different, protein specific, life-times. Also, the time courses of SARS CoV-2 spike protein after mRNA Covid vaccination should follow the predicted behavior although in different timescales [129,130]. For future mRNA-based therapies, that follow rational design strategies for combinatorial therapies, the delivery of multiple protein and RNAs will become important. We showed that consideration of timelines in codelivery of multiple species is potentially complex, not necessarily strictly synchronized and dependent on physical–chemical properties of the different nucleic acid components. Firstly, the molar packing efficiency in codelivery is an open problem. Secondly, very little is known about the fate of nucleic acids in the time window after endosomal escape and before measurable action, like GFP expression. We would like to call this time window the dark hour of transfection (see Fig. 1). Modern single molecule fluorescent techniques could bring light into mechanisms of mRNA release from remaining ionizable lipid, the intracellular transport and degradation processes and the details of codon-specific binding and processing via ribosomes. The challenge is the detection of rare events, since, only a small fraction of LNP particles and mRNA molecules are active, as well as the detection of correlations that could elicit the mode of action. To this end it will be crucial to develop novel fluorescent probes, that signal the state of the mRNA or the microenvironment as well as automated image analysis tools that detect correlations and rare events. In principle, combinatorial delivery based on RNA-LNPs could be extended to a larger number of different nucleic acid components. LNP formulations are compatible with nucleic acid molecules in general, including pDNA, mRNA, siRNA as well as sgRNA. Multiple synthetic nucleic acid molecules enable the execution of transiently expressed synthetic circuits and open the possibility of LNP based synthetic biology [58]. Regulation of mRNA life-time via micro-RNAs is a prominent motif in natural gene regulation, correspondingly complex synthetic gene manipulation via LNP mediated RNA delivery should be feasible. Moreover, RNAs that interfere with gene circuits at multiple anchor points will allow for enhanced, highly specific and even personalized combinatorial gene therapies. Kinetic modelling of LNP delivery and expression is a prerequisite for a reliable system-level prediction of gene expression response and will be a guiding tool for future precision engineering of therapeutic options.

Credit authorship contribution statement

Judith A. Müller: Conceptualization, Formal analysis, Writing – original draft, Writing – review & editing. **Nathalie Schäffler:** Visualization, Writing – original draft. **Thomas Kellerer:** Software, Writing – original draft. **Gerlinde Schwake:** Methodology, Supervision, Validation. **Thomas S. Ligon:** Software, Writing – original draft. **Joachim O. Rädler:** Conceptualization, Funding acquisition, Supervision, Writing – original draft, Writing – review & editing.

Declaration of competing interest

The authors declare that they have no known competing financial interests or personal relationships that could have appeared to influence the work reported in this paper.

Data availability

Data will be made available on request.

Acknowledgments

This work was funded by the Deutsche Forschungsgemeinschaft (DFG, German Research Foundation) – Project-ID 201269156 – SFB

1032-B01 as well as by the Federal Ministry of Education and Research (BMBF) and the Free State of Bavaria under the Excellence Strategy of the Federal Government and the Länder through the ONE MUNICH Project Munich Multiscale Biofabrication. Support by a grant from the Bayerische Forschungsstiftung is gratefully acknowledged. T.K. acknowledges funding through BMBF, Germany Projekt FKZ13N16300.

References

[1] H. Yin, R.L. Kanasty, A.A. Eltoukhy, A.J. Vegas, J.R. Dorkin, D.G. Anderson, Non-viral vectors for gene-based therapy, Nat Rev Genet 15 (2014) 541–555, https://doi.org/10.1038/nrg3763.
[2] P.R. Cullis, M.J. Hope, Lipid Nanoparticle Systems for Enabling Gene Therapies, Mol. Ther. 25 (2017) 1467–1475, https://doi.org/10.1016/j.ymthe.2017.03.013.
[3] A.N. Kuhn, T. Beißert, P. Simon, B. Vallazza, J. Buck, B.P. Davies, O. Tureci, U. Sahin, mRNA as a Versatile Tool for Exogenous Protein Expression, 12 (2012). Doi: 10.2174/156652312802762536.
[4] E. Kon, N. Ad-El, I. Hazan-Halevy, L. Stotsky-Oterin, D. Peer, Targeting cancer with mRNA–lipid nanoparticles: key considerations and future prospects, Nat Rev Clin Oncol (2023), https://doi.org/10.1038/s41571-023-00811-9.
[5] S. Kreiter, M. Diken, A. Selmi, Ö. Türeci, U. Sahin, Tumor vaccination using messenger RNA: prospects of a future therapy, Curr. Opin. Immunol. 23 (2011) 399–406, https://doi.org/10.1016/j.coi.2011.03.007.
[6] J.G. Rurik, I. Tombácz, A. Yadegari, P.O.M. Fernández, S.V. Shewale, L. Li, T. Kimura, O.Y. Soliman, T.E. Papp, Y.K. Tam, B.L. Mui, S.M. Albelda, E. Puré, C.H. June, H. Aghajanian, D. Weissman, H. Parhiz, J.A. Epstein, CAR T cells produced in vivo to treat cardiac injury, (2022).
[7] J.D. Finn, A.R. Smith, M.C. Patel, L. Shaw, M.R. Youniss, J. Van Heteren, T. Dirstine, C. Ciullo, R. Lescarbeau, J. Seitzer, R.R. Shah, A. Shah, D. Ling, J. Growe, M. Pink, E. Rohde, K.M. Wood, W.E. Salomon, W.F. Harrington, C. Dombrowski, W.R. Strapps, Y. Chang, D.V. Morrissey, A Single Administration of CRISPR/Cas9 Lipid Nanoparticles Achieves Robust and Persistent In Vivo Genome Editing, Cell Rep. 22 (2018) 2227–2235, https://doi.org/10.1016/j.celrep.2018.02.014.
[8] S.C. Semple, A. Akinc, J. Chen, A.P. Sandhu, B.L. Mui, C.K. Cho, D.W.Y. Sah, D. Stebbing, E.J. Crosley, E. Yaworski, I.M. Hafez, J.R. Dorkin, J. Qin, K. Lam, K. G. Rajeev, K.F. Wong, L.B. Jeffs, L. Nechev, M.L. Eisenhardt, M. Jayaraman, M. Kazem, M.A. Maier, M. Srinivasulu, M.J. Weinstein, Q. Chen, R. Alvarez, S. A. Barros, S. De, S.K. Klimuk, T. Borland, V. Kosovrasti, W.L. Cantley, Y.K. Tam, M. Manoharan, M.A. Ciufolini, M.A. Tracy, A. De Fougerolles, I. MacLachlan, P. R. Cullis, T.D. Madden, M.J. Hope, Rational design of cationic lipids for siRNA delivery, Nat Biotechnol 28 (2010) 172–176, https://doi.org/10.1038/nbt.1602.
[9] X. Hou, T. Zaks, R. Langer, Y. Dong, Lipid nanoparticles for mRNA delivery, Nat Rev Mater 6 (2021) 1078–1094, https://doi.org/10.1038/s41578-021-00358-0.
[10] A. Akinc, A. Zumbuehl, M. Goldberg, E.S. Leshchiner, V. Busini, N. Hossain, S. A. Bacallado, D.N. Nguyen, J. Fuller, R. Alvarez, A. Borodovsky, T. Borland, R. Constien, A. De Fougerolles, J.R. Dorkin, K. Narayanannair Jayaprakash, M. Jayaraman, M. John, V. Koteliansky, M. Manoharan, L. Nechev, J. Qin, T. Racie, D. Raitcheva, K.G. Rajeev, D.W.Y. Sah, J. Soutschek, I. Toudjarska, H.-P. Vornlocher, T.S. Zimmermann, R. Langer, D.G. Anderson, A combinatorial library of lipid-like materials for delivery of RNAi therapeutics, Nat Biotechnol 26 (2008) 561–569, https://doi.org/10.1038/nbt1402.
[11] A.K.K. Leung, I.M. Hafez, S. Baoukina, N.M. Belliveau, I.V. Zhigaltsev, E. Afshinmanesh, D.P. Tieleman, C.L. Hansen, M.J. Hope, P.R. Cullis, Lipid Nanoparticles Containing siRNA Synthesized by Microfluidic Mixing Exhibit an Electron-Dense Nanostructured Core, J. Phys. Chem. C 116 (2012) 18440–18450, https://doi.org/10.1021/jp303267y.
[12] M. Yanez Arteta, T. Kjellman, S. Bartesaghi, S. Wallin, X. Wu, A.J. Kvist, A. Dabkowska, N. Székely, A. Radulescu, J. Bergenholtz, L. Lindfors, Successful reprogramming of cellular protein production through mRNA delivered by functionalized lipid nanoparticles, Proc. Natl. Acad. Sci. U.S.A. 115 (2018), https://doi.org/10.1073/pnas.1720542115.
[13] M.A. Maier, M. Jayaraman, S. Matsuda, J. Liu, S. Barros, W. Querbes, Y.K. Tam, S. M. Ansell, V. Kumar, J. Qin, X. Zhang, Q. Wang, S. Panesar, R. Hutabarat, M. Carioto, J. Hettinger, P. Kandasamy, D. Butler, K.G. Rajeev, B. Pang, K. Charisse, K. Fitzgerald, B.L. Mui, X. Du, P. Cullis, T.D. Madden, M.J. Hope, M. Manoharan, A. Akinc, Biodegradable Lipids Enabling Rapidly Eliminated Lipid Nanoparticles for Systemic Delivery of RNAi Therapeutics, Mol. Ther. 21 (2013) 1570–1578, https://doi.org/10.1038/mt.2013.124.
[14] D. Adams, A. Gonzalez-Duarte, W.D. O'Riordan, C.-C. Yang, M. Ueda, A. V. Kristen, I. Tournev, H.H. Schmidt, T. Coelho, J.L. Berk, K.-P. Lin, G. Vita, S. Attarian, V. Planté-Bordeneuve, M.M. Mezei, J.M. Campistol, J. Buades, T. H. Brannagan, B.J. Kim, J. Oh, Y. Parman, Y. Sekijima, P.N. Hawkins, S. D. Solomon, M. Polydefkis, P.J. Dyck, P.J. Gandhi, S. Goyal, J. Chen, A.L. Strahs, S.V. Nochur, M.T. Sweetser, P.P. Garg, A.K. Vaishnaw, J.A. Gollob, O.B. Suhr, Patisiran, an RNAi Therapeutic, for Hereditary Transthyretin Amyloidosis, N Engl J Med 379 (2018) 11–21, https://doi.org/10.1056/NEJMoa1716153.
[15] Y. Dong, D.J. Siegwart, D.G. Anderson, Strategies, design, and chemistry in siRNA delivery systems, Adv. Drug Deliv. Rev. 144 (2019) 133–147, https://doi.org/10.1016/j.addr.2019.05.004.
[16] N. Pardi, S. Tuyishime, H. Muramatsu, K. Kariko, B.L. Mui, Y.K. Tam, T. D. Madden, M.J. Hope, D. Weissman, Expression kinetics of nucleoside-modified mRNA delivered in lipid nanoparticles to mice by various routes, J. Control. Release 217 (2015) 345–351, https://doi.org/10.1016/j.jconrel.2015.08.007.
[17] A.-T. Dinh, C. Pangarkar, T. Theofanous, S. Mitragotri, Understanding Intracellular Transport Processes Pertinent to Synthetic Gene Delivery via Stochastic Simulations and Sensitivity Analyses, Biophys. J. 92 (2007) 831–846, https://doi.org/10.1529/biophysj.106.095521.
[18] C. Leonhardt, G. Schwake, T.R. Stögbauer, S. Rappl, J.-T. Kuhr, T.S. Ligon, J. O. Rädler, Single-cell mRNA transfection studies: Delivery, kinetics and statistics by numbers, Nanomed.: Nanotechnol. Biol. Med. 10 (2014) 679–688, https://doi.org/10.1016/j.nano.2013.11.008.
[19] C.M. Varga, K. Hong, D.A. Lauffenburger, Quantitative Analysis of Synthetic Gene Delivery Vector Design Properties, Mol. Ther. 4 (2001) 438–446, https://doi.org/10.1006/mthe.2001.0475.
[20] H. Kamiya, H. Akita, H. Harashima, Pharmacokinetic and pharmacodynamic considerations in gene therapy, Drug Discov. Today 8 (2003) 990–996, https://doi.org/10.1016/S1359-6446(03)02889-7.
[21] T.S. Ligon, C. Leonhardt, J.O. Rädler, Multi-Level Kinetic Model of mRNA Delivery via Transfection of Lipoplexes, PLoS One 9 (2014) e107148.
[22] X. Zhang, V. Goel, G.J. Robbie, Pharmacokinetics of Patisiran, the First Approved RNA Interference Therapy in Patients With Hereditary Transthyretin-Mediated Amyloidosis, J. Clin. Pharma 60 (2020) 573–585, https://doi.org/10.1002/jcph.1553.
[23] C. Lorenz, M. Fotin-Mleczek, G. Roth, C. Becker, T.C. Dam, W.P.R. Verdurmen, R. Brock, J. Probst, T. Schlake, Protein expression from exogenous mRNA: Uptake by receptor-mediated endocytosis and trafficking via the lysosomal pathway, RNA Biol. 8 (2011) 627–636, https://doi.org/10.4161/rna.8.4.15394.
[24] B. Snijder, L. Pelkmans, Origins of regulated cell-to-cell variability, Nat Rev Mol Cell Biol 12 (2011) 119–125, https://doi.org/10.1038/nrm3044.
[25] S.J. Altschuler, L.F. Wu, Cellular Heterogeneity: Do Differences Make a Difference? Cell 141 (2010) 559–563, https://doi.org/10.1016/j.cell.2010.04.033.
[26] A. Murschhauser, P.J.F. Röttgermann, D. Woschée, M.F. Ober, Y. Yan, K. A. Dawson, J.O. Rädler, A high-throughput microscopy method for single-cell analysis of event-time correlations in nanoparticle-induced cell death, Commun Biol 2 (2019) 35, https://doi.org/10.1038/s42003-019-0282-0.
[27] L. Zheng, S.R. Bandara, Z. Tan, C. Leal, Lipid Nanoparticle topology regulates endosomal escape and delivery of RNA to the cytoplasm, PNAS 120 (2023) 10, https://doi.org/10.1073/pnas.2301067120.
[28] J.C.W. Locke, M.B. Elowitz, Using movies to analyse gene circuit dynamics in single cells, Nat Rev Microbiol 7 (2009) 383–392, https://doi.org/10.1038/nrmicro2056.
[29] Y. Shav-Tal, R.H. Singer, X. Darzacq, Imaging gene expression in single living cells, Nat Rev Mol Cell Biol 5 (2004) 855–862, https://doi.org/10.1038/nrm1494.
[30] R.Y. Tsien, THE GREEN FLUORESCENT PROTEIN, Annu. Rev. Biochem. 67 (1998) 509–544, https://doi.org/10.1146/annurev.biochem.67.1.509.
[31] R. Heim, R.Y. Tsien, Engineering green fluorescent protein for improved brightness, longer wavelengths and fluorescence resonance energy transfer, Curr. Biol. 6 (1996) 178–182, https://doi.org/10.1016/S0960-9822(02)00450-5.
[32] B.C. Campbell, E.M. Nabel, M.H. Murdock, C. Lao-Peregrin, P. Tsoulfas, M. G. Blackmore, F.S. Lee, C. Liston, H. Morishita, G.A. Petsko, mGreenLantern: a bright monomeric fluorescent protein with rapid expression and cell filling properties for neuronal imaging, Proc. Natl. Acad. Sci. U.S.A. 117 (2020) 30710–30721, https://doi.org/10.1073/pnas.2000942117.
[33] T.W.J. Gadella, L. Van Weeren, J. Stouthamer, M.A. Hink, A.H.G. Wolters, B.N. G. Giepmans, S. Aumonier, J. Dupuy, A. Royant, mScarlet3: a brilliant and fast-maturing red fluorescent protein, Nat Methods 20 (2023) 541–545, https://doi.org/10.1038/s41592-023-01809-y.
[34] J.L. Kirschman, S. Bhosle, D. Vanover, E.L. Blanchard, K.H. Loomis, C. Zurla, K. Murray, B.C. Lam, P.J. Santangelo, Characterizing exogenous mRNA delivery, trafficking, cytoplasmic release and RNA–protein correlations at the level of single cells, Nucleic Acids Res. 45 (2017) e113–e, https://doi.org/10.1093/nar/gkx290.
[35] K. Rombouts, K. Braeckmans, K. Remaut, Fluorescent Labeling of Plasmid DNA and mRNA: Gains and Losses of Current Labeling Strategies, Bioconjugate Chem. 27 (2016) 280–297, https://doi.org/10.1021/acs.bioconjchem.5b00579.
[36] A. Reiser, D. Woschée, S.M. Kempe, J.O. Rädler, Live-cell Imaging of Single-Cell Arrays (LISCA) - a Versatile Technique to Quantify Cellular Kinetics, J vis Exp (2021), https://doi.org/10.3791/62025.
[37] R. Krzysztoń, D. Woschée, A. Reiser, G. Schwake, H.H. Strey, J.O. Rädler, Single-cell kinetics of siRNA-mediated mRNA degradation, Nanomedicine: Nanotechnology, Biology and Medicine 21 (2019) 102077, https://doi.org/10.1016/j.nano.2019.102077.
[38] J.A. Müller, G. Schwake, J.O. Rädler, Einzelzellmikroskopie im Hochdurchsatz auf Mikrostrukturen, BIOspektrum 28 (2022) 723–725, https://doi.org/10.1007/s12268-022-1857-8.
[39] S. Hou, C. Johnson, K. Welsher, Real-Time 3D Single Particle Tracking: Towards Active Feedback Single Molecule Spectroscopy in Live Cells, Molecules 24 (2019) 2826, https://doi.org/10.3390/molecules24152826.
[40] B. Brandenburg, X. Zhuang, Virus trafficking – learning from single-virus tracking, Nat Rev Microbiol 5 (2007) 197–208, https://doi.org/10.1038/nrmicro1615.
[41] S.-L. Liu, Z.-G. Wang, H.-Y. Xie, A.-A. Liu, D.C. Lamb, D.-W. Pang, Single-Virus Tracking: From Imaging Methodologies to Virological Applications, Chem. Rev. 120 (2020) 1936–1979, https://doi.org/10.1021/acs.chemrev.9b00692.

[42] S. Patel, N. Ashwanikumar, E. Robinson, Y. Xia, C. Mihai, J.P. Griffith, S. Hou, A. A. Esposito, T. Ketova, K. Welsher, J.L. Joyal, Ö. Almarsson, G. Sahay, Naturally-occurring cholesterol analogues in lipid nanoparticles induce polymorphic shape and enhance intracellular delivery of mRNA, Nat Commun 11 (2020) 983, https://doi.org/10.1038/s41467-020-14527-2.
[43] A.J. Rozo, M.H. Cox, A. Devitt, A.J. Rothnie, A.D. Goddard, Biophysical analysis of lipidic nanoparticles, Methods 180 (2020) 45–55, https://doi.org/10.1016/j.ymeth.2020.05.001.
[44] N. Ruthardt, D.C. Lamb, C. Bräuchle, Single-particle Tracking as a Quantitative Microscopy-based Approach to Unravel Cell Entry Mechanisms of Viruses and Pharmaceutical Nanoparticles, Mol. Ther. 19 (2011) 1199–1211, https://doi.org/10.1038/mt.2011.102.
[45] N. Korabel, A. Taloni, G. Pagnini, V. Allan, S. Fedotov, T.A. Waigh, Ensemble heterogeneity mimics ageing for endosomal dynamics within eukaryotic cells, Sci Rep 13 (2023) 8789, https://doi.org/10.1038/s41598-023-35903-0.
[46] S. Ben Djemaa, K. Hervé-Aubert, L. Lajoie, A. Falanga, S. Galdiero, S. Nedellec, M. Soucé, E. Munnier, I. Chourpa, S. David, E. Allard-Vannier, gH625 Cell-Penetrating Peptide Promotes the Endosomal Escape of Nanovectorized siRNA in a Triple-Negative Breast Cancer Cell Line, Biomacromolecules 20 (2019) 3076–3086, https://doi.org/10.1021/acs.biomac.9b00637.
[47] Z. Cheng, G. Teo, S. Krueger, T.M. Rock, H.W. Koh, H. Choi, C. Vogel, Differential dynamics of the mammalian mRNA and protein expression response to misfolding stress, Mol. Syst. Biol. 12 (2016) 855, https://doi.org/10.15252/msb.20156423.
[48] L. Shang, P. Gao, H. Wang, R. Popescu, D. Gerthsen, G.U. Nienhaus, Protein-based fluorescent nanoparticles for super-resolution STED imaging of live cells, Chem. Sci. 8 (2017) 2396–2400, https://doi.org/10.1039/C6SC04664A.
[49] T. Andrian, R. Riera, S. Pujals, L. Albertazzi, Nanoscopy for endosomal escape quantification, Nanoscale Adv. 3 (2021) 10–23, https://doi.org/10.1039/D0NA00454E.
[50] M.Y. Berezin, S. Achilefu, Fluorescence Lifetime Measurements and Biological Imaging, Chem. Rev. 110 (2010) 2641–2684, https://doi.org/10.1021/cr900343z.
[51] T. Kellerer, J. Janusch, C. Freymüller, A. Rühm, R. Sroka, T. Hellerer, Comprehensive Investigation of Parameters Influencing Fluorescence Lifetime Imaging Microscopy in Frequency- and Time-Domain Illustrated by Phasor Plot Analysis, IJMS 23 (2022) 15885, https://doi.org/10.3390/ijms232415885.
[52] J.J. Rennick, C.J. Nowell, C.W. Pouton, A.P.R. Johnston, Resolving subcellular pH with a quantitative fluorescent lifetime biosensor, Nat Commun 13 (2022) 6023, https://doi.org/10.1038/s41467-022-33348-z.
[53] R. Datta, T.M. Heaster, J.T. Sharick, A.A. Gillette, M.C. Skala, Fluorescence lifetime imaging microscopy: fundamentals and advances in instrumentation, analysis, and applications, J. Biomed. Opt. 25 (2020) 1, https://doi.org/10.1117/1.JBO.25.7.071203.
[54] T.h. Förster, Zwischenmolekulare Energiewanderung und Fluoreszenz, Ann. Phys. 437 (1948) 55–75, https://doi.org/10.1002/andp.19484370105.
[55] T. Chen, B. He, J. Tao, Y. He, H. Deng, X. Wang, Y. Zheng, Application of Förster Resonance Energy Transfer (FRET) technique to elucidate intracellular and In Vivo biofate of nanomedicines, Adv. Drug Deliv. Rev. 143 (2019) 177–205, https://doi.org/10.1016/j.addr.2019.04.009.
[56] L. Loura, FRET in membrane biophysics: an overview, Front. Physio. 2 (2011), https://doi.org/10.3389/fphys.2011.00082.
[57] M. Ferizi, C. Leonhardt, C. Meggle, M.K. Aneja, C. Rudolph, C. Plank, J.O. Rädler, Stability analysis of chemically modified mRNA using micropattern-based single-cell arrays, Lab Chip 15 (2015) 3561–3571, https://doi.org/10.1039/C5LC00749F.
[58] T. Frei, F. Cella, F. Tedeschi, J. Gutiérrez, G.-B. Stan, M. Khammash, V. Siciliano, Characterization and mitigation of gene expression burden in mammalian cells, Nat Commun 11 (2020) 4641, https://doi.org/10.1038/s41467-020-18392-x.
[59] G. Sahay, D.Y. Alakhova, A.V. Kabanov, Endocytosis of nanomedicines, J. Control. Release 145 (2010) 182–195, https://doi.org/10.1016/j.jconrel.2010.01.036.
[60] J. Gilleron, W. Querbes, A. Zeigerer, A. Borodovsky, G. Marsico, U. Schubert, K. Manygoats, S. Seifert, C. Andree, M. Stöter, H. Epstein-Barash, L. Zhang, V. Koteliansky, K. Fitzgerald, E. Fava, M. Bickle, Y. Kalaidzidis, A. Akinc, M. Maier, M. Zerial, Image-based analysis of lipid nanoparticle–mediated siRNA delivery, intracellular trafficking and endosomal escape, Nat Biotechnol 31 (2013) 638–646, https://doi.org/10.1038/nbt.2612.
[61] D. Manzanares, V. Ceña, Endocytosis: The Nanoparticle and Submicron Nanocompounds Gateway into the Cell, Pharmaceutics 12 (2020) 371, https://doi.org/10.3390/pharmaceutics12040371.
[62] J.J. Rennick, A.P.R. Johnston, R.G. Parton, Key principles and methods for studying the endocytosis of biological and nanoparticle therapeutics, Nat. Nanotechnol. 16 (2021) 266–276, https://doi.org/10.1038/s41565-021-00858-8.
[63] J. Rejman, A. Bragonzi, M. Conese, Role of clathrin- and caveolae-mediated endocytosis in gene transfer mediated by lipo- and polyplexes, Mol. Ther. 12 (2005) 468–474, https://doi.org/10.1016/j.ymthe.2005.03.038.
[64] K. Von Gersdorff, N.N. Sanders, R. Vandenbroucke, S.C. De Smedt, E. Wagner, M. Ogris, The Internalization Route Resulting in Successful Gene Expression Depends on both Cell Line and Polyethylenimine Polyplex Type, Mol. Ther. 14 (2006) 745–753, https://doi.org/10.1016/j.ymthe.2006.07.006.
[65] S. Behzadi, V. Serpooshan, W. Tao, M.A. Hamaly, M.Y. Alkawareek, E.C. Dreaden, D. Brown, A.M. Alkilany, O.C. Farokhzad, M. Mahmoudi, Cellular uptake of nanoparticles: journey inside the cell, Chem. Soc. Rev. 46 (2017) 4218–4244, https://doi.org/10.1039/C6CS00636A.
[66] A. Akinc, W. Querbes, S. De, J. Qin, M. Frank-Kamenetsky, K.N. Jayaprakash, M. Jayaraman, K.G. Rajeev, W.L. Cantley, J.R. Dorkin, J.S. Butler, L. Qin, T. Racie, A. Sprague, E. Fava, A. Zeigerer, M.J. Hope, M. Zerial, D.W. Sah, K. Fitzgerald, M.A. Tracy, M. Manoharan, V. Koteliansky, A.D. Fougerolles, M. A. Maier, Targeted Delivery of RNAi Therapeutics With Endogenous and Exogenous Ligand-Based Mechanisms, Mol. Ther. 18 (2010) 1357–1364, https://doi.org/10.1038/mt.2010.85.
[67] K. Liu, R. Nilsson, E. Lázaro-Ibáñez, H. Duàn, T. Miliotis, M. Strimfors, M. Lerche, A.R. Salgado Ribeiro, J. Ulander, D. Lindén, A. Salvati, A. Sabirsh, Multiomics analysis of naturally efficacious lipid nanoparticle coronas reveals high-density lipoprotein is necessary for their function, Nat Commun 14 (2023) 4007, https://doi.org/10.1038/s41467-023-39768-9.
[68] N. Aliakbarinodehi, A. Gallud, M. Mapar, E. Wesén, S. Heydari, Y. Jing, G. Emilsson, K. Liu, A. Sabirsh, V.P. Zhdanov, L. Lindfors, E.K. Esbjörner, F. Höök, Interaction Kinetics of Individual mRNA-Containing Lipid Nanoparticles with an Endosomal Membrane Mimic: Dependence on pH, Protein Corona Formation, and Lipoprotein Depletion, ACS Nano 16 (2022) 20163–20173, https://doi.org/10.1021/acsnano.2c04829.
[69] L. Miao, J. Lin, Y. Huang, L. Li, D. Delcassian, Y. Ge, Y. Shi, D.G. Anderson, Synergistic lipid compositions for albumin receptor mediated delivery of mRNA to the liver, Nat Commun 11 (2020) 2424, https://doi.org/10.1038/s41467-020-16248-y.
[70] V. Francia, R.M. Schiffelers, P.R. Cullis, D. Witzigmann, The Biomolecular Corona of Lipid Nanoparticles for Gene Therapy, Bioconjugate Chem. 31 (2020) 2046–2059, https://doi.org/10.1021/acs.bioconjchem.0c00366.
[71] D. Zhu, H. Yan, Z. Zhou, J. Tang, X. Liu, R. Hartmann, W.J. Parak, N. Feliu, Y. Shen, Detailed investigation on how the protein corona modulates the physicochemical properties and gene delivery of polyethylenimine (PEI) polyplexes, Biomater. Sci. 6 (2018) 1800–1817, https://doi.org/10.1039/C8BM00128F.
[72] E. Álvarez-Benedicto, Z. Tian, S. Chatterjee, D. Orlando, M. Kim, E.D. Guerrero, X. Wang, D.J. Siegwart, Spleen SORT LNP Generated in situ CAR T Cells Extend Survival in a Mouse Model of Lymphoreplete B Cell Lymphoma, Angew Chem Int Ed 62 (2023) e202310395.
[73] I. Tombácz, D. Laczkó, H. Shahnawaz, H. Muramatsu, A. Natesan, A. Yadegari, T. E. Papp, M.-G. Alameh, V. Shuvaev, B.L. Mui, Y.K. Tam, V. Muzykantov, N. Pardi, D. Weissman, H. Parhiz, Highly efficient CD4+ T cell targeting and genetic recombination using engineered CD4+ cell-homing mRNA-LNPs, Mol. Ther. 29 (2021) 3293–3304, https://doi.org/10.1016/j.ymthe.2021.06.004.
[74] H. Parhiz, V.V. Shuvaev, N. Pardi, M. Khoshnejad, R.Y. Kiseleva, J.S. Brenner, T. Uhler, S. Tuyishime, B.L. Mui, Y.K. Tam, T.D. Madden, M.J. Hope, D. Weissman, V.R. Muzykantov, PECAM-1 directed re-targeting of exogenous mRNA providing two orders of magnitude enhancement of vascular delivery and expression in lungs independent of apolipoprotein E-mediated uptake, J. Control. Release 291 (2018) 106–115, https://doi.org/10.1016/j.jconrel.2018.10.015.
[75] A. Gallud, M.J. Munson, K. Liu, A. Idström, H.M.G. Barriga, S.R. Tabaei, N. Aliakbarinodehi, M. Ojansivu, Q. Lubart, J.J. Doutch, M.N. Holme, L. Evenäs, L. Lindfors, M.M. Stevens, A. Collén, A. Sabirsh, F. Höök, E.K. Esbjörner, Time evolution of PEG-shedding and serum protein coronation determines the cell uptake kinetics and delivery of lipid nanoparticle formulated mRNA, Biophysics (2021), https://doi.org/10.1101/2021.08.20.457104.
[76] J.E. Dahlman, K.J. Kauffman, Y. Xing, T.E. Shaw, F.F. Mir, C.C. Dlott, R. Langer, D.G. Anderson, E.T. Wang, Barcoded nanoparticles for high throughput in vivo discovery of targeted therapeutics, Proc. Natl. Acad. Sci. U.S.A. 114 (2017) 2060–2065, https://doi.org/10.1073/pnas.1620874114.
[77] M.J. Munson, G. O'Driscoll, A.M. Silva, E. Lázaro-Ibáñez, A. Gallud, J.T. Wilson, A. Collén, E.K. Esbjörner, A. Sabirsh, A high-throughput Galectin-9 imaging assay for quantifying nanoparticle uptake, endosomal escape and functional RNA delivery, Commun Biol 4 (2021) 211, https://doi.org/10.1038/s42003-021-01728-8.
[78] D.S. Dimitrov, Virus entry: molecular mechanisms and biomedical applications, Nat Rev Microbiol 2 (2004) 109–122, https://doi.org/10.1038/nrmicro817.
[79] P. Paramasivam, C. Franke, M. Stöter, A. Höijer, S. Bartesaghi, A. Sabirsh, L. Lindfors, M.Y. Arteta, A. Dahlén, A. Bak, S. Andersson, Y. Kalaidzidis, M. Bickle, M. Zerial, Endosomal escape of delivered mRNA from endosomal recycling tubules visualized at the nanoscale, J. Cell Biol. 221 (2022) e202110137.
[80] S.E.A. Gratton, P.A. Ropp, P.D. Pohlhaus, J.C. Luft, V.J. Madden, M.E. Napier, J. M. DeSimone, The effect of particle design on cellular internalization pathways, Proc. Natl. Acad. Sci. U.S.A. 105 (2008) 11613–11618, https://doi.org/10.1073/pnas.0801763105.
[81] J. Rejman, V. Oberle, I.S. Zuhorn, D. Hoekstra, Size-dependent internalization of particles via the pathways of clathrin- and caveolae-mediated endocytosis, Biochem. J 377 (2004) 159–169, https://doi.org/10.1042/bj20031253.
[82] H. Yuan, J. Li, G. Bao, S. Zhang, Variable Nanoparticle-Cell Adhesion Strength Regulates Cellular Uptake, Phys. Rev. Lett. 105 (2010) 138101, https://doi.org/10.1103/PhysRevLett.105.138101.
[83] S.K. Lai, K. Hida, C. Chen, J. Hanes, Characterization of the intracellular dynamics of a non-degradative pathway accessed by polymer nanoparticles, J. Control. Release 125 (2008) 107–111, https://doi.org/10.1016/j.jconrel.2007.10.015.
[84] K.J. Hassett, J. Higgins, A. Woods, B. Levy, Y. Xia, C.J. Hsiao, E. Acosta, Ö. Almarsson, M.J. Moore, L.A. Brito, Impact of lipid nanoparticle size on mRNA vaccine immunogenicity, J. Control. Release 335 (2021) 237–246, https://doi.org/10.1016/j.jconrel.2021.05.021.

[85] S. Cao, X. Liu, X. Li, C. Lin, W. Zhang, C.H. Tan, S. Liang, B. Luo, X. Xu, P.E. Saw, Shape Matters: Comprehensive Analysis of Star-Shaped Lipid Nanoparticles, Front. Pharmacol. 11 (2020) 539, https://doi.org/10.3389/fphar.2020.00539.

[86] A. Wittrup, A. Ai, X. Liu, P. Hamar, R. Trifonova, K. Charisse, M. Manoharan, T. Kirchhausen, J. Lieberman, Visualizing lipid-formulated siRNA release from endosomes and target gene knockdown, Nat Biotechnol 33 (2015) 870–876, https://doi.org/10.1038/nbt.3298.

[87] M.P. Dobay, A. Schmidt, E. Mendoza, T. Bein, J.O. Rädler, Cell Type Determines the Light-Induced Endosomal Escape Kinetics of Multifunctional Mesoporous Silica Nanoparticles, Nano Lett. 13 (2013) 1047–1052, https://doi.org/10.1021/nl304273u.

[88] E.J. Sayers, S.E. Peel, A. Schantz, R.M. England, M. Beano, S.M. Bates, A.S. Desai, S. Puri, M.B. Ashford, A.T. Jones, Endocytic Profiling of Cancer Cell Models Reveals Critical Factors Influencing LNP-Mediated mRNA Delivery and Protein Expression, Mol. Ther. 27 (2019) 1950–1962, https://doi.org/10.1016/j.ymthe.2019.07.018.

[89] S. Patel, N. Ashwanikumar, E. Robinson, A. DuRoss, C. Sun, K.E. Murphy-Benenato, C. Mihai, Ö. Almarsson, G. Sahay, Boosting Intracellular Delivery of Lipid Nanoparticle-Encapsulated mRNA, Nano Lett. 17 (2017) 5711–5718, https://doi.org/10.1021/acs.nanolett.7b02664.

[90] A. Parodi, C. Corbo, A. Cevenini, R. Molinaro, R. Palomba, L. Pandolfi, M. Agostini, F. Salvatore, E. Tasciotti, Enabling cytoplasmic delivery and organelle targeting by surface modification of nanocarriers, Nanomedicine 10 (2015) 1923–1940, https://doi.org/10.2217/nnm.15.39.

[91] I.M.S. Degors, C. Wang, Z.U. Rehman, I.S. Zuhorn, Carriers Break Barriers in Drug Delivery: Endocytosis and Endosomal Escape of Gene Delivery Vectors, Acc. Chem. Res. 52 (2019) 1750–1760, https://doi.org/10.1021/acs.accounts.9b00177.

[92] K.V. Kilchrist, S.C. Dimobi, M.A. Jackson, B.C. Evans, T.A. Werfel, E.A. Dailing, S. K. Bedingfield, I.B. Kelly, C.L. Duvall, Gal8 Visualization of Endosome Disruption Predicts Carrier-Mediated Biologic Drug Intracellular Bioavailability, ACS Nano (2019), https://doi.org/10.1021/acsnano.8b05482 acsnano.8b05482.

[93] M. Maugeri, M. Nawaz, A. Papadimitriou, A. Angerfors, A. Camponeschi, M. Na, M. Hölttä, P. Skantze, S. Johansson, M. Sundqvist, J. Lindquist, T. Kjellman, I.-L. Mårtensson, T. Jin, P. Sunnerhagen, S. Östman, L. Lindfors, H. Valadi, Linkage between endosomal escape of LNP-mRNA and loading into EVs for transport to other cells, Nat Commun 10 (2019) 4333, https://doi.org/10.1038/s41467-019-12275-6.

[94] S. Sabnis, E.S. Kumarasinghe, T. Salerno, C. Mihai, T. Ketova, J.J. Senn, A. Lynn, A. Bulychev, I. McFadyen, J. Chan, Ö. Almarsson, M.G. Stanton, K.E. Benenato, A Novel Amino Lipid Series for mRNA Delivery: Improved Endosomal Escape and Sustained Pharmacology and Safety in Non-human Primates, Mol. Ther. 26 (2018) 1509–1519, https://doi.org/10.1016/j.ymthe.2018.03.010.

[95] H. Zhang, J. Bussmann, F.H. Huhnke, J. Devoldere, A. Minnaert, W. Jiskoot, F. Serwane, J. Spatz, M. Röding, S.C. De Smedt, K. Braeckmans, K. Remaut, Together is Better: mRNA Co-Encapsulation in Lipoplexes is Required to Obtain Ratiometric Co-Delivery and Protein Expression on the Single Cell Level, Adv. Sci. 9 (2022) 2102072, https://doi.org/10.1002/advs.202102072.

[96] M. Schlich, R. Palomba, G. Costabile, S. Mizrahy, M. Pannuzzo, D. Peer, P. Decuzzi, Cytosolic delivery of nucleic acids: The case of ionizable lipid nanoparticles, Bioeng Transl Med 6 (2021), https://doi.org/10.1002/btm2.10213.

[97] J.O. Rädler, I. Koltover, T. Salditt, C.R. Safinya, Structure of DNA-Cationic Liposome Complexes: DNA Intercalation in Multilamellar Membranes in Distinct Interhelical Packing Regimes, Science 275 (1997) 810–814, https://doi.org/10.1126/science.275.5301.810.

[98] I. Koltover, T. Salditt, J.O. Rädler, C.R. Safinya, An Inverted Hexagonal Phase of Cationic Liposome-DNA Complexes Related to DNA Release and Delivery, Science 281 (1998) 78–81, https://doi.org/10.1126/science.281.5373.78.

[99] H.M.G. Barriga, O. Ces, R.V. Law, J.M. Seddon, N.J. Brooks, Engineering Swollen Cubosomes Using Cholesterol and Anionic Lipids, Langmuir 35 (2019) 16521–16527, https://doi.org/10.1021/acs.langmuir.9b02336.

[100] Z. Li, J. Carter, L. Santos, C. Webster, C.F. Van Der Walle, P. Li, S.E. Rogers, J. R. Lu, Acidification-Induced Structure Evolution of Lipid Nanoparticles Correlates with Their *In Vitro* Gene Transfections, ACS Nano 17 (2023) 979–990, https://doi.org/10.1021/acsnano.2c06213.

[101] H. Yu, A. Angelova, B. Angelov, B. Dyett, L. Matthews, Y. Zhang, M. El Mohamad, X. Cai, S. Valimehr, C.J. Drummond, J. Zhai, Real-Time pH-Dependent Self-Assembly of Ionisable Lipids from COVID-19 Vaccines and In Situ Nucleic Acid Complexation, Angew Chem Int Ed 62 (2023) e202304977.

[102] J. Philipp, A. Dabkowska, A. Reiser, K. Frank, R. Krzysztoń, C. Brummer, B. Nickel, C.E. Blanchet, A. Sudarsan, M. Ibrahim, S. Johansson, P. Skantze, U. Skantze, S. Östman, M. Johansson, N. Henderson, K. Elvevold, B. Smedsrød, N. Schwierz, L. Lindfors, J.O. Rädler, pH-dependent structural transitions in cationic ionizable lipid mesophases are critical for lipid nanoparticle function, PNAS (2023).

[103] M.R. Hunter, L. Cui, B.T. Porebski, S. Pereira, S. Sonzini, U. Odunze, P. Iyer, O. Engkvist, R.L. Lloyd, S. Peel, A. Sabirsh, D. Ross-Thriepland, A.T. Jones, A. S. Desai, Understanding Intracellular Biology to Improve mRNA Delivery by Lipid Nanoparticles, Small, Methods (2023) 2201695, https://doi.org/10.1002/smtd.202201695.

[104] B. Li, X. Luo, B. Deng, J. Wang, D.W. McComb, Y. Shi, K.M.L. Gaensler, X. Tan, A. L. Dunn, B.A. Kerlin, Y. Dong, An Orthogonal Array Optimization of Lipid-like Nanoparticles for mRNA Delivery in Vivo, Nano Lett. 15 (2015) 8099–8107, https://doi.org/10.1021/acs.nanolett.5b03528.

[105] J. Zhang, R. Xue, W.-Y. Ong, P. Chen, Roles of Cholesterol in Vesicle Fusion and Motion, Biophys. J. 97 (2009) 1371–1380, https://doi.org/10.1016/j.bpj.2009.06.025.

[106] C.M. Bailey-Hytholt, G. Ulinski, J. Dugas, M. Haines, M. Lazebnik, P. Piepenhagen, I.E. Zarraga, A. Bandekar, Intracellular trafficking kinetics of nucleic acid escape from lipid nanoparticles via fluorescence imaging, CPB 24 (2023), https://doi.org/10.2174/1389201024666230403094238.

[107] J. Nguyen, F.C. Szoka, Nucleic Acid Delivery: The Missing Pieces of the Puzzle? Acc. Chem. Res. 45 (2012) 1153–1162, https://doi.org/10.1021/ar3000162.

[108] L.M.P. Vermeulen, T. Brans, S.K. Samal, P. Dubruel, J. Demeester, S.C. De Smedt, K. Remaut, K. Braeckmans, Endosomal Size and Membrane Leakiness Influence Proton Sponge-Based Rupture of Endosomal Vesicles, ACS Nano 12 (2018) 2332–2345, https://doi.org/10.1021/acsnano.7b07583.

[109] C. Peetla, S. Jin, J. Weimer, A. Elegbede, V. Labhasetwar, Biomechanics and Thermodynamics of Nanoparticle Interactions with Plasma and Endosomal Membrane Lipids in Cellular Uptake and Endosomal Escape, Langmuir 30 (2014) 7522–7532, https://doi.org/10.1021/la5015219.

[110] A. Reiser, D. Woschée, N. Mehrotra, R. Krzysztoń, H.H. Strey, J.O. Rädler, Correlation of mRNA delivery timing and protein expression in lipid-based transfection, Integr. Biol. 11 (2019) 362–371, https://doi.org/10.1093/intbio/zyz030.

[111] R.L. Ball, K.A. Hajj, J. Vizelman, P. Bajaj, K.A. Whitehead, Lipid Nanoparticle Formulations for Enhanced Co-delivery of siRNA and mRNA, Nano Lett. 18 (2018) 3814–3822, https://doi.org/10.1021/acs.nanolett.8b01101.

[112] A.G. Hamilton, K.L. Swingle, R.A. Joseph, D. Mai, N. Gong, M.M. Billingsley, M. Alameh, D. Weissman, N.C. Sheppard, C.H. June, M.J. Mitchell, Ionizable Lipid Nanoparticles with Integrated Immune Checkpoint Inhibition for mRNA CAR T Cell Engineering, Adv Healthcare Materials (2023) 2301515, https://doi.org/10.1002/adhm.202301515.

[113] Y. Zhu, R. Shen, I. Vuong, R.A. Reynolds, M.J. Shears, Z.-C. Yao, Y. Hu, W.J. Cho, J. Kong, S.K. Reddy, S.C. Murphy, H.-Q. Mao, Multi-step screening of DNA/lipid nanoparticles and co-delivery with siRNA to enhance and prolong gene expression, Nat Commun 13 (2022) 4282, https://doi.org/10.1038/s41467-022-31993-y.

[114] C.L. Xu, M.Z.C. Ruan, V.B. Mahajan, S.H. Tsang, Viral Delivery Systems for CRISPR, Viruses 11 (2019) 28, https://doi.org/10.3390/v11010028.

[115] W.L. Chew, M. Tabebordbar, J.K.W. Cheng, P. Mali, E.Y. Wu, A.H.M. Ng, K. Zhu, A.J. Wagers, G.M. Church, A multifunctional AAV–CRISPR–Cas9 and its host response, Nat Methods 13 (2016) 868–874, https://doi.org/10.1038/nmeth.3993.

[116] G. Ronzitti, D.-A. Gross, F. Mingozzi, Human Immune Responses to Adeno-Associated Virus (AAV) Vectors, Front. Immunol. 11 (2020) 670, https://doi.org/10.3389/fimmu.2020.00670.

[117] T. Wei, Q. Cheng, Y.-L. Min, E.N. Olson, D.J. Siegwart, Systemic nanoparticle delivery of CRISPR-Cas9 ribonucleoproteins for effective tissue specific genome editing, Nat Commun 11 (2020) 3232, https://doi.org/10.1038/s41467-020-17029-3.

[118] J.B. Miller, S. Zhang, P. Kos, H. Xiong, K. Zhou, S.S. Perelman, H. Zhu, D.J. Siegwart, Non-viral CRISPR/Cas gene editing in vitro and in vivo enabled by synthetic nanoparticle co-delivery of Cas9 mRNA and sgRNA, (2018).

[119] J.P. Han, M. Kim, B.S. Choi, J.H. Lee, G.S. Lee, M. Jeong, Y. Lee, E.-A. Kim, H.-K. Oh, N. Go, H. Lee, K.J. Lee, U.G. Kim, J.Y. Lee, S. Kim, J. Chang, H. Lee, D. W. Song, S.C. Yeom, In vivo delivery of CRISPR-Cas9 using lipid nanoparticles enables antithrombin gene editing for sustainable hemophilia A and B therapy, Sci. Adv. 8 (2022) eabj6901, https://doi.org/10.1126/sciadv.abj6901.

[120] D. Rosenblum, A. Gutkin, R. Kedmi, S. Ramishetti, N. Veiga, A.M. Jacobi, M. S. Schubert, D. Friedmann-Morvinski, Z.R. Cohen, M.A. Behlke, J. Lieberman, D. Peer, CRISPR-Cas9 genome editing using targeted lipid nanoparticles for cancer therapy, Sci. Adv. 6 (2020) eabc9450, https://doi.org/10.1126/sciadv.abc9450.

[121] K. Lee, M. Conboy, H.M. Park, F. Jiang, H.J. Kim, M.A. Dewitt, V.A. Mackley, K. Chang, A. Rao, C. Skinner, T. Shobha, M. Mehdipour, H. Liu, W. Huang, F. Lan, N.L. Bray, S. Li, J.E. Corn, K. Kataoka, J.A. Doudna, I. Conboy, N. Murthy, Nanoparticle delivery of Cas9 ribonucleoprotein and donor DNA in vivo induces homology-directed DNA repair, Nat Biomed Eng 1 (2017) 889–901, https://doi.org/10.1038/s41551-017-0137-2.

[122] G. Schwake, S. Youssef, J.-T. Kuhr, S. Gude, M.P. David, E. Mendoza, E. Frey, J. O. RÄdler, Predictive modeling of non-viral gene transfer, Biotechnol. Bioeng. (2010), https://doi.org/10.1002/bit.22604.

[123] J.R. Melamed, K.A. Hajj, N. Chaudhary, D. Strelkova, M.L. Arral, N. Pardi, M.-G. Alameh, J.B. Miller, L. Farbiak, D.J. Siegwart, D. Weissman, K.A. Whitehead, Lipid nanoparticle chemistry determines how nucleoside base modifications alter mRNA delivery, J. Control. Release 341 (2022) 206–214, https://doi.org/10.1016/j.jconrel.2021.11.022.

[124] C.A. Lino, J.C. Harper, J.P. Carney, J.A. Timlin, Delivering CRISPR: a review of the challenges and approaches, Drug Deliv. 25 (2018) 1234–1257, https://doi.org/10.1080/10717544.2018.1474964.

[125] L. Duan, K. Ouyang, X. Xu, L. Xu, C. Wen, X. Zhou, Z. Qin, Z. Xu, W. Sun, Y. Liang, Nanoparticle Delivery of CRISPR/Cas9 for Genome Editing, Front. Genet. 12 (2021) 673286, https://doi.org/10.3389/fgene.2021.673286.

[126] F.J. Khan, G. Yuen, J. Luo, Multiplexed CRISPR/Cas9 gene knockout with simple crRNA:tracrRNA co-transfection, Cell Biosci 9 (2019) 41, https://doi.org/10.1186/s13578-019-0304-0.

[127] L.L. Lesueur, L.M. Mir, F.M. André, Overcoming the Specific Toxicity of Large Plasmids Electrotransfer in Primary Cells In Vitro, Mol. Ther. Nucleic Acids 5 (2016) e291.

[128] U. Sahin, K. Karikó, Ö. Türeci, mRNA-based therapeutics — developing a new class of drugs, Nat Rev Drug Discov 13 (2014) 759–780, https://doi.org/10.1038/nrd4278.

[129] K.J. Hassett, K.E. Benenato, E. Jacquinet, A. Lee, A. Woods, O. Yuzhakov, S. Himansu, J. Deterling, B.M. Geilich, T. Ketova, C. Mihai, A. Lynn, I. McFadyen, M.J. Moore, J.J. Senn, M.G. Stanton, Ö. Almarsson, G. Ciaramella, L.A. Brito, Optimization of Lipid Nanoparticles for Intramuscular Administration of mRNA Vaccines, Mol. Ther. Nucleic Acids 15 (2019) 1–11, https://doi.org/10.1016/j.omtn.2019.01.013.

[130] C.-Y. Wu, C.-W. Cheng, C.-C. Kung, K.-S. Liao, J.-T. Jan, C. Ma, C.-H. Wong, Glycosite-deleted mRNA of SARS-CoV-2 spike protein as a broad-spectrum vaccine, Proc. Natl. Acad. Sci. U.S.A. 119 (2022), https://doi.org/10.1073/pnas.2119995119 e2119995119.

[131] P.C.N. Rensen, L.A.J.M. Sliedregt, M. Ferns, E. Kieviet, S.M.W. Van Rossenberg, S. H. Van Leeuwen, T.J.C. Van Berkel, E.A.L. Biessen, Determination of the Upper Size Limit for Uptake and Processing of Ligands by the Asialoglycoprotein Receptor on Hepatocytesin Vitro and in Vivo, J. Biol. Chem. 276 (2001) 37577–37584, https://doi.org/10.1074/jbc.M101786200.